Near-Highway Aerosol and Gas-phase Measurements in a High Diesel Environment

DeWitt H.L.[1], Hellebust S.[1], Temime-Roussel B.[1], Ravier S.[1], Polo L.[2,3], Jacob V. [2], Buisson C., Charron A.[3], André M. [3], Pasquier A.[3], Besombes J.L.[4], Jaffrezo J.L.[2], Wortham H.[1], Marchand N.[1]

[1]Aix Marseille Université, CNRS, LCE FRE 3416, 13331 Marseille, France
[2] Université Grenoble Alpes, CNRS, LGGE, F-38000 Grenoble, France
[3] IFSTTAR, Case 24, 69675 Bron Cédex, France
[4] Université de Savoie, LCME, 73376 Le Bourget du lac, France

Corresponding authors: H. Langley DeWitt (Helen-Langley.Dewitt@univ-amu.fr) and Nicolas Marchand (Nicolas.Marchand@univ-amu.fr).

Abstract

Diesel-powered passenger cars currently outnumber gasoline-powered cars in many countries, particularly in Europe. In France, diesel cars represented 61% of light duty vehicles in 2011 and this percentage is still increasing (French Environment and Energy Management Agency, ADEME). As part of the September 2011 joint PM-DRIVE (Particulate Matter- DiRect and Indirect on-road Vehicular Emissions) and MOCOPO (Measuring and mOdeling traffic COngestion and POllution) field campaign, the concentration and high-resolution chemical composition of aerosols and volatile organic carbon (VOC) species were measured adjacent to a major urban highway south of Grenoble, France. Alongside these atmospheric measurements, detailed traffic data were collected from nearby traffic cameras and loop detectors, which allowed the vehicle type, traffic concentration, and traffic speed to be quantified. Six aerosol age and source profiles were resolved using the positive matrix factorization (PMF) model on real-time high-resolution aerosol mass spectra. These six aerosol source/age categories included a hydrocarbon-like organic aerosol (HOA) commonly associated with primary vehicular emissions, a nitrogen containing aerosol (NOA) with a diurnal pattern similar to that of HOA, oxidized organic aerosol (OOA), and biomass burning aerosol (BBOA). While quantitatively separating influence of diesel versus gasoline proved impossible, a low HOA: Black Carbon ratio, similar to that measured in other high-diesel environments, and high levels of NOx, also indicative of diesel emissions, were observed. Although the measurement site was located next to a large source of primary emissions, which are typically found to have low oxygen incorporation, OOA was found to comprise the majority of the measured organic aerosol, and isotopic analysis showed that the measured OOA contained mainly modern carbon, not fossil-derived carbon. Thus, even in this heavily vehicular-emission impacted environment, photochemical processes, biogenic emissions, and aerosol oxidation

55 dominated the overall organic aerosol mass measured during most of the campaign.

56 **1. Introduction**

57 Aerosols are known to have adverse effects on human health and on the global climate. The
58 World Health Organization (WHO) recently added anthropogenic aerosol and air pollution to their list
59 of known carcinogens (WHO, 2013), and high mass concentrations of particles less than 2.5
60 micrometers in diameter (PM2.5), such as those emitted by vehicular combustion processes, are
61 particularly harmful (Lighty et al., 2000)**.** Vehicular traffic is a large source of submicrometer
62 anthropogenic aerosol and proximity to large sources of vehicular emissions has been shown to
63 increase lung and heart disease, especially in children (Brugge et al., 2007). A recent WHO report
64 examined the toxilogical effects of black carbon (BC) aerosol, a known emission of diesel vehicles.
65 Although no difference in toxicology between PM2.5 and BC aerosol inhalation was found, BC was
66 cited as a marker for more general vehicular emissions, which have been shown to have negative health
67 effects; diesel exhaust was added as a known carcinogen the year before general air pollution and
68 PM2.5 (Janssen, World Health Organization, 2012). Aside from the potential detrimental health
69 effects of BC, BC also has significant implications for climate change. Unlike the majority of aerosol
70 (e.g., most organic aerosol, ammonium sulfate, ammonium nitrate), BC aerosol is associated with
71 global warming due to its high absorption of solar radiation (Bond et al., 2013). Diesel vehicles have
72 been singled out as important sources of BC to regulate as, unlike most other BC sources, diesel
73 vehicles tend not to co-elute high concentrations of other, less absorbing (thus more cooling) aerosol
74 and therefore have a higher net heating effect than mixed-emission black carbon sources (Bond et al.,
75 2013).

76 In France, the lower cost of diesel fuel (due to a lower taxation rate of diesel fuel versus
77 gasoline fuel) and the generally higher fuel efficiency of diesel engines have increased the popularity of
78 diesel passenger cars. In 2011, 82% of the fuel consumed in France was diesel (World Bank, 2011).
79 For comparison, this percentage in 2011 was 28% in the US, 57% in China, 70% in the European

Union, 49% in Latin America and the Middle East, and 83% in low-income countries.

The emission characteristics and emission limits of these two types of engines (diesel and gasoline) are quite different: diesel vehicles have higher emission factors for primary organic aerosol (POA) and BC, while gasoline-powered vehicles have higher emission factors for carbon monoxide (CO), carbon dioxide (CO_2), and volatile organic carbon (VOCs) (e.g., trimethylbenzene, benzene) (Platt et al., 2013). Black carbon, in particular, is closely associated with diesel: in Europe, North America, and Latin America, an estimated 70% of BC emissions are from diesel-powered vehicles (Bond et al., 2013). In Marseille, France, a traffic tunnel experiment measured an organic carbon/elemental carbon ratio (OC/EC) in PM2.5 of 0.3-0.4, which indicates that significant amounts of black carbon is emitted from local traffic in Marseille (El Haddad et al., 2009). Recent measures have been taken in Europe to reduce the particulate emission from diesel vehicles: from Euro 4 to Euro 5, a diesel particle filter (DPF) was introduced in diesel vehicles and the regulated emission limit for PM2.5 was halved for diesel cars and trucks.

Aerosol and VOC emissions from both vehicle types, as well as biogenic emissions, industrial emissions, and emissions from other sources, will react together in the atmosphere and potentially form secondary organic aerosol (SOA). Thus, primary aerosol emissions may not be the most important emission factor to take into account for global reduction in anthropogenic aerosol. After emission, VOCs can react in the atmosphere and form SOA. From these reactions, gasoline VOC emissions could ultimately lead to the formation of higher concentrations of organic aerosol than organic aerosol released directly from diesel vehicles, as reported in a recent study comparing the SOA formation from a Euro 3 diesel LDV and a Euro 5 gasoline LDV (Platt et al., 2013).

A recent study by Bahreini et al. (2012) measured similar levels of SOA in the heavily traffic-influenced LA Basin during both weekend and weekday afternoons. While diesel-powered vehicle numbers on the road decrease significantly on the weekends in the LA area, the measured SOA does not, which leads to the conclusion that gasoline emissions are more responsible for SOA than diesel

105 emissions (Bahreini et al., 2012). Nordin et al. (2013) performed smog-chamber studies on SOA
106 formation from gasoline-vehicle VOC emissions during simulated cold start and idling driving
107 conditions, and confirmed the high potential of SOA formation from gasoline car exhaust. Another
108 recent paper calculates the reactivity potential of diesel and gasoline fuel and comes to the opposite
109 conclusion: that due to the reactivity potential of diesel fuel, diesel-powered vehicles should contribute
110 greater amounts of SOA than gasoline-powered vehicles to the atmosphere (Gentner et al., 2012). Thus,
111 controversy still exists regarding the eventual aerosol emission factors of diesel and gasoline engines
112 when considering both primary emissions and potential SOA formation.

113 Finally, gas-phase NO and NO_2 (NOx) ambient concentrations are also mostly associated with
114 diesel fuel use (Vestreng et al., 2009). Throughout Europe, while NOx emission standards for diesel
115 vehicles have increased in stringency in recent years, ambient NO_2 levels have not shown a
116 corresponding decrease (Vestreng et al., 2009). The reduction of atmospheric NOx is important for
117 health-related reasons as an increase in NOx leads to an increase in tropospheric ozone, which is a
118 known lung irritant. NOx levels have also been shown to affect the formation rate, formation pathways,
119 and chemical composition of secondary organic aerosol from the reaction of primary species in
120 numerous chamber studies (Carlton et al., 2009; Kroll et al., 2005; Ng et al., 2007, 2008; Presto et al.,
121 2010).

122 European vehicular emissions, near-highway pollution levels, and the chemical composition of
123 highway pollution may be quite different than those measured in North America due to many factors,
124 including: 1) different emission standards and fuel regulations in the two regions 2) different after-
125 treatment devices to reduce the emission of certain pollutants and 3) a much larger percentage of
126 diesel-powered passenger cars on the road. A comparison between European and North American
127 near-highway measurements could lead to further understanding of the effects of diesel versus gasoline
128 on near-highway atmospheric chemistry.

129 To fully categorize the aerosol, VOC, and NOx emissions of traffic in France, the joint PM-

DRIVE (Particulate Matter- DiRect and Indirect on-road Vehicular Emissions) and MOCOPO (Measuring and mOdeling traffic COngestion and POllution) field mission took place in the Grenoble basin, France during the fall of 2011 at a near-highway location south of the city center. During the field measurements discussed in this paper, traffic cameras allowed vehicle type determination through license plate automatic identification. Traffic densities, speed and total flow were quantified through loop detectors, while measurements of the chemical composition, concentration, and size of aerosol were collected using both real-time and offline analysis, and parallel data on the gas-phase chemical composition of the roadway-adjacent environment were also collected. A source apportionment model was applied to real-time aerosol chemical composition data. Particular attention was paid to the chemical composition of particles and VOCs emitted during morning and evening rush hours in an attempt to elucidate the primary vehicular influence on near-highway air pollution.

2. Experimental Methods

2.1. Description of the Measurement Site

The sampling site was located at 45.150641 N, 5.726028 E (Figure 1), just south of Grenoble, France adjacent to a major highway (south of E712, with A480 2 km to the east). During the week, the total traffic on the highway was about 95,000 vehicles day^{-1} (65,000 during the weekend). Grenoble, a large city with over half a million people, is located in the southeast of France at the foothills of the Alps. The surrounding mountain ranges both buffer the Grenoble area from the effects of transported aerosol and can also trap pollution within the valley, particularly during the winter months and periods of temperature inversions. The isolating effect of the mountains thus simplifies the potential sources for aerosol, making it an interesting location for the study of specific aerosol emission sources.

2.2. Traffic Cameras and Loop Detectors

Traffic cameras mounted to a roadway sign were used to capture the license plate numbers of vehicles driven on the highway close to the field measurement site. These numbers were later used to classify vehicular traffic into different categories: vehicle type (LDV, Heavy duty vehicles (HDV),

buses) and age, vehicle size and engine capacity, fuel type (diesel or gasoline), and Euro number (i.e. the pollutant emission regulation that the vehicle complies with), The speed of the passing vehicles was also monitored with the classical traffic detector (double electromagnetic loops, able to identify the passing of all vehicles and their speeds), which allowed the identification of periods of stop-and-go, dense, or free-flow traffic.

2.3. Massalya Platform

The MASSALYA platform is a mobile laboratory equipped for air quality measurements with a hub located at the Aix Marseille Université. For the field campaign, PM2.5 and PM1 sampling heads situated above the roof of the stationary truck were connected to a variety of online instrumentation located within the truck body. Complementary off-line analysis was performed on filter samples collected by HiVol samplers located adjacent to the MASSALYA platform. All sampling occurred approximately 15 m from one of the traffic lines, as shown in Figure 1. Further details can be found in Polo-Rehn, (2013).

A High-Resolution Time-of-Flight Aerosol Mass Spectrometer (Aerodyne, HR-ToF-AMS) was used to analyze the chemical composition, size, and concentration of non-refractory submicrometer particles in the ambient atmosphere (DeCarlo et al., 2006). Instrument specifications have been discussed in detail elsewhere (DeCarlo et al., 2006). Briefly, both high resolution and size-speciated chemical information for ambient aerosol were obtained from this instrument. Aerosols were vaporized at 600 ^{o}C, ionized using electron ionization (EI) at an energy of 70 eV, and the chemical composition of bulk aerosol was measured using a ToF mass spectrometer (TOFWERK). Aerosol spectra were continuously collected and a two-minute average spectrum was obtained. Aerosol vacuum aerodynamic diameter was calculated by setting a particle start time using a chopper wheel and measuring the particle flight time along the particle ToF (pToF) sizing region (DeCarlo et al., 2006). Typical resolution during the campaign was around 2800 m/Δm (where m=*m/z* and Δm=full-width at half max of the mass peak).

In addition to the HR-ToF-AMS, a Size-Mobility Particle Scanner (TSI, SMPS) was used to measure the size distribution and concentration of ambient aerosol and a Multiangle Absorption Photometer (Thermofischer, MAAP 5012) was used to measure the concentration of black carbon.

High resolution mass spectra of VOCs were obtained using an Ionicon Proton-Transfer Reaction Time of Flight Mass Spectrometer 8000 (PTR-ToF-MS, hereafter referred to as PTR-MS) (Graus et al., 2010). The PTR-MS analyzes trace (parts per trillion by volume) VOCs with high mass resolution, which allows the separation of different species with the same nominal mass and the identification of each peak's elemental formula. The PTR-MS was run with a 25 second time resolution and a flow of 100 cm^3 min^{-1}. Drift tube parameters of the PTR-MS were as follows: Voltage: 560 V, Drift tube pressure: 2.11 mbar, Drift tube temperature: 333 K, resulting in an E/N (electric field/number concentration of neutral particles) of 133 Td.

The SMPS, PTR-ToF-MS, and HR-ToF-AMS were connected to the same sample inlet with a PM2.5 sampling head and a sample flow of 1 m^3 hr^{-1}. Particles were dried (RH<30%) using a Nafion dryer prior to measurement with the HR-ToF-AMS and SMPS. The MAAP was connected to a separate PM1 sampling head. PM1 filter HiVol (30 m^3 h^{-1}) samples were collected on quartz filters (Tissuquartz) on a daily basis and analyzed for radiocarbon isotope data. Radiocarbon measurements were conducted using ARTEMIS Accelerator Mass Spectrometry, at Saclay (CNRS-CEA-IRD-IRSN, France) on the total carbon (TC) fraction after a combustion of the samples at 850°C. The method is fully described in El Haddad et al. (2011).

A Young meteorological station was also installed to capture wind speed, wind direction, relative humidity, and temperature data at the measurement location.

2.4. Air Rhône Alpes station

Twenty meters east of the Massalya platform, still adjacent to the highway, the Air Rhône Alps station collected PM2.5 HiVol (30 m^3 h^{-1}) samples on quartz fiber filters (Tissuquartz) with a time

205 resolution of 4 hours. PM2.5 samples were analyzed for EC/OC, inorganic ions, and targeted organic
206 tracers (Polo-Rehn, 2013).
207 Organic compounds in these PM samples were also quantified by gas chromatography coupled
208 with mass spectrometry (GC-MS), following the method detailed in El Haddad et al. (2009) and Favez
209 et al. (2010). EC and OC measurements were performed using the Thermo-Optical Transmission (TOT)
210 method on a Sunset Lab analyzer (Birch and Cary, 1996; Jaffrezo et al., 2005) following the
211 EUSAAR2 temperature program (Cavalli et al., 2010). Ionic species were analyzed with Ionic
212 Chromatography (IC) following the method described in Jaffrezo et al. (1998).
213 All filters used in this study were preheated at 500 ^{o}C during 3 h. Samples were stored at -18 ^{o}C
214 in aluminum foil and sealed in polyethylene bags until analysis.
215 In addition, NOx (NO and NO_2), PM10 and PM2.5 mass concentrations were measured and a
216 Tapered Element Oscillating Microbalance equipped with a Filter Dynamic Measurement System
217 (TEOM-FDMS, Thermo Scientific) for real-time measurements of PM10 and PM2.5.
218 **3. Results and Discussion**
219 *3.1 Traffic Conditions at the Measurement Site*

220 A detailed view of the measured traffic is presented in the supplementary information (Figure
221 S1). Briefly, the overall makeup of the traffic remained fairly steady throughout the campaign. The
222 bulk of the vehicles directly affecting the measurement site were Euro 4 (released in 2005) or older;
223 thus, the most recent emission regulations had only a small effect on the air quality around the field site.
224 The ratio between diesel and gasoline cars was found to be 2.6, or 72% diesel, with a high correlation
225 (R^2=0.96) between diesel and gasoline vehicles.
226 *3.2. General atmospheric conditions and aerosol and VOC concentrations and evolution*
227 Wind speeds were generally low throughout the campaign (<1-2 m/s) with higher wind speeds
228 peaking in the afternoons and tapering off in the evenings. The wind direction was primarily from the

229 northwest, from the direction of the nearby highway. A diagram of the two measurement stations, the
230 wind rose plot for the Massalya location, and polar plots showing the concentration of NO and BC as a
231 function of wind direction are shown in Figure 1. BC and NO were associated with all wind directions,
232 though slightly higher from the highway direction, which suggested that the measurement site was
233 influenced by both traffic emissions and also often by regional, traffic-influenced background air
234 masses. In order to better describe the traffic influence, we defined high traffic periods (HT) within the
235 dataset. These HT periods were selected as follows : wind direction >40 or <320, NO in the 75^{th}
236 percentile, and from 6:30-9:30 or 17:00-20:00 (rush hour periods). The fixed location of the
237 measurement stations made determination of concentration drop-off as a function of distance from the
238 roadway impossible to determine with the dataset, although that has been shown to be important in
239 other studies (such as Karner et al., 2010). However, the measurements were all taken closer to the
240 roadway (~15 m) than the calculated distance where roadway emission drop off to background levels
241 (115-570 m, Karner et al., 2010).
242 The campaign time series concentration of submicrometer non-refractory aerosol sulfate (SO_4),
243 ammonium (NH_4), nitrate (NO_3), and organic species from the HR-ToF-AMS is shown in Figure 2A.
244 The limit of detection for each species was calculated using the method described byDeCarlo et al.
245 (2006) and found to be 0.30, 0.21, 0.06, and 0.33 μg m^{-3} for SO_4, NH_4, NO_3, and organic aerosol,
246 respectively, for our measurements with a time resolution of 2.5 min. A collection efficiency (CE) of
247 0.75 was applied to HR-ToF-AMS aerosol concentration measurements taken during this campaign.
248 The CE factor compensates for incomplete vaporization of non-refractory species due to particle
249 bounce, the likelihood of which changes with particle phase and chemical speciation (Huffman et al.,
250 2005; Matthew et al., 2008). This CE was calculated by comparing the HR-ToF-AMS SO_4
251 concentrations to 4 hour filter concentrations (Figure S2). This comparison gave a value of 0.75±0.03
252 for the slope between the two types of measurements.

PM2.5 averaged 17 μg m^{-3} for the campaign (Figure S3) while PM10 averaged 22 μg m^{-3}. These values increased slightly during HT periods (a 1.3 and 1.25x increase, respectively). Black carbon and organic aerosol species dominated the measured aerosol composition throughout the campaign, and comprised 39 and 40% of the total speciated submicrometer aerosol, respectively. PM2.5 had a somewhat higher mass variation than the AMS + BC measured mass (Figure S3), likely due to the smaller measurement size cutoff for AMS (1 μm) and the presence of road dust in the local environment, a large portion of which may be non-refractory and thus unable to be measured by the AMS. Increases in BC and the aerosol marker *m/z* 57 ($C_4H_9^+$), a marker for primary organic carbon in the HR-ToF-AMS (Zhang et al., 2005), correlated in time to the observed morning and evening traffic peaks (Figure 2B), with BC levels reaching 10-16 μg m^{-3} during the mornings (Figure 2A) for 2.5 min averaged measurements. As expected, an increase of BC and m/z 57 (1.5x) was observed during HT periods. Note that BC concentrations during high filter loadings (BC accumulation rate > 0.14 μg min^{-1}) have been removed to compensate for the underestimation of BC by the MAAP during periods of high concentrations (Hyvärinen et al., 2013). Along with increased concentrations of *m/z* 57 and BC, elevated number concentrations of small particles (up to 1-2x10^5 cm^{-3} during peaks from daily base levels of 2-4x10^4 cm^{-3}) were observed during periods of HT (Figure 2D), for 5 min measurements. BC and *m/z* 57 had similar daily averages throughout the campaign; however, overall organic concentration rose significantly during the period from 9/12-9/14, when particle growth events were observed (Figure 2D). The geometric number mode diameter rose over the course of each day to a maximum diameter each afternoon, when photochemical processing was the most intense. A marker for oxidized, aged organic aerosol (Figure 2C, *m/z* 44, COO^+) also rose in concentration during this time period, further confirming that the larger aerosol and higher organic mass concentrations were due to aging and secondary organic aerosol formation processes. A period of heavy rain on the 18th and 19th of September removed much of the organic aerosol from the local atmosphere. Black carbon

277 concentrations and small particle concentrations quickly returned to their previous levels. A new
278 accumulation period was observed after rainfall (Figure 2D), with the mode diameter of particles
279 increasing as secondary aerosol was formed again. The slow rise of organic concentration during these
280 periods, the lower BC:Org ratio, the enhancement of organic concentration outside of normal traffic
281 periods, and the low level of NO during these accumulation periods all suggest that this increase in
282 organic aerosol concentration was driven by regional influences, not by nearby vehicular emissions and
283 a more southerly wind direction during this time confirmed the transport of non-highway air masses to
284 the measurement site.

285 These findings are similar to those presented recently by Sun et al., (2012), who measured
286 aerosol size and chemical composition adjacent to the Long Island Expressway in New York and
287 observed that traffic-influenced aerosol emissions were primarily small particles which varied in
288 concentration with changes in traffic throughout the day. During periods with less traffic influence,
289 more oxygenated organic aerosol (OOA) and inorganic ions with larger mode diameters and lower
290 temporal variations were observed (Sun et al., 2012).

291 The time series concentrations of selected VOC peaks are shown in Figure 3. Primary traffic
292 related VOC species, such as aromatics (benzene and trimethylbenzene), were found to have high
293 temporal variations similar to those of traffic-related aerosol species and NOx (Figure 4C and D). NOx
294 levels were often over 400 ppbv during the morning rush hours, while the PTRMS peak corresponding
295 (in part) to toluene and benzene peaked around 2 to 1 ppbv (respectively). During a recent chamber
296 study in Ispra, Italy, fresh diesel emissions PTR-MS VOC spectra were found to contain peaks with the
297 same mass as $CH_4NO_2^+$ and $C_2H_5O^+$ (Hellebust et al., 2013, 2015), not present in fresh gasoline
298 emissions. These same peaks were also observed during this work and found to vary with traffic
299 during this measurement period, but had a smoother variation than the observed aromatics (Figure 3B).
300 While this species is unique for fresh diesel emissions versus gasoline emissions, aging processes occur
301 rapidly and other sources may contribute to this mass peak. Thus, these species, while increasing with

traffic, cannot be assumed to be tracers for primary diesel emissions in particular; no high-concentration unique tracer peak for diesel VOC emissions was resolved from the fresh diesel emission spectra in these chamber experiments (Hellebust et al., 2015). A slight increase of the traffic related VOCs (1.2x for benzene and trimethylbenzene) was observed during HT periods compared to the campaign average. For $CH_4NO_2^+$ this relative increase during HT periods is lower (8%), which could confirm multiple sources of this compound.

In addition to traffic-related VOC emissions, mass peaks corresponding in exact mass to biogenic emissions, such as isoprene, were measured in ppbv levels. These peaks were found to rise in concentration with the ambient temperature (Figure 3A), typical of isoprene peaks. The presence of isoprene and its oxidation product, methyl vinyl ketone (MVK) or its isomer methacrolein (MACR), in similar concentrations as that of the major traffic-related VOC peaks (ppbv levels) suggested that biogenic emissions also significantly influenced the local atmosphere despite close proximity to anthropogenic emission sources (i.e., road traffic).

The high morning concentrations of traffic-related pollutants, compared to evening concentrations, were caused in part by a low early morning boundary layer that rose during the day and fell during the night. Boundary layer heights (BLH) were estimated using the Hybrid Single Particle Lagrangian Integrated Trajectory (HYSPLIT) backtrajectory model. The HYSPLIT model either extracts the BLH from meteorological file input into the model or, if no BLH exists in the meteorological file, BLH is estimated using the vertical temperature profile. A selection of the BLH-scaled diurnal profiles of traffic and biogenic emission related VOC concentrations are shown in Figure 4A along with traffic (speed, vehicular flux) diurnal profiles and the calculated boundary layer heights and measured temperatures (Figure 4B and C). This calculation was performed to more directly compare vehicle concentration and speed to vehicular emissions and temperature with biogenic emissions (by removing the dilution of emissions by the changing boundary layer height). Biogenic species, such as isoprene, peaked in concentration during the afternoon, when temperatures were the

warmest. Aromatic species peaked in concentration, even after the rough boundary layer correction was applied, during periods of low speeds. This is consistent with other findings that show cold starts and idling speeds cause an increase in aromatic VOC emissions from gasoline-powered vehicles (e.g., Broderick and Marnane, 2002).

3.3 PMF Analysis

The positive matrix factorization (PMF) model was applied to the HR-ToF-AMS aerosol data using the process described in detail by Ulbrich et al. (2009). Six aerosol factors were resolved by their source and relative aging using the PMF model: a hydrocarbon-like organic aerosol (HOA) factor, a regional oxidized organic aerosol (OOA-Reg) factor associated with sulfate aerosol, two oxidized organic aerosol factors with opposing diurnal patterns, one more oxidized than the other (Less Oxidized Organic Aerosol, or LO-OA, with peak concentration during the mornings/nights, and More Oxidized Organic Aerosol, or MO-OA, with peak concentrations during the afternoons), a biomass-burning organic aerosol factor (BBOA), and a nitrogen-containing organic aerosol factor (NOA). The mass spectra for the six resolved factors is shown in Figure 5, labeled with their identifications. Evaluation graphs for the six-factor PMF solution are shown in the Supplementary Information (Figures S5-S8). Polar plots of the factor concentrations and wind direction are shown in Figure S9. A six factor solution was the lowest number of factors where a BBOA factor was resolved; BBOA was suspected to be present in the air mass measured during the campaign due to periods of increased levoglucosan measured on filter samples. However, its concentrations were very low (15 ng m^{-3} on average, Polo-Rehn, (2013)) compared to concentrations measured in Grenoble in winter (around 800 $ng.m^{-3}$ (Herich et al., 2014)). Solutions with more than six factors appeared to split the OOA factor further until differences between each OOA factor were difficult to justify. The calculated elemental ratios of O:C, H:C, and Organic Mass: Organic Carbon (OM:OC), (Aiken et al., 2008) are shown in Table 1.

352 The diurnal pattern and the relative concentrations of each resolved factor, averaged over the
353 campaign period, are shown in Figure 6, along with the standard deviation of their concentrations.
354 Morning and evening peaks, correlating in time to rush hour traffic, were clearly observable for the
355 HOA factor. Also clearly visible in Figure 6A is the opposing diurnal trends of LO-OA (peaking at
356 night and early morning) and MO-OA (peaking around 3pm each afternoon). OOA-Reg had no
357 discernable diurnal trend. An interesting finding in these data is that the HOA and NOA factor
358 concentrations both peaked during morning and evening high traffic periods (Figure 6A). This is not
359 the general behavior demonstrated in most studies for the NOA factor, although a similar NOA factor
360 has been previously measured in the Po Valley, Italy (Saarikoski et al., 2012). This behavior was
361 confirmed by examining HT periods, with an increase of 1.3x and 1.9x for NOA and HOA
362 concentrations, respectively, during HT periods. While many of the defined N-containing peaks were
363 adjacent to or in between those of larger hydrocarbons or of other organics, only N-containing peaks
364 whose fitting significantly reduced the residual mass at each unit mass were fit (Figure S8).
365 Additionally, and when possible, the w-ToF mode data was examined to determine if the N-containing
366 peak was resolved enough from neighboring peaks for certain identification.
367 In Figure 7, the time series of each factor are shown with oxalate ($C_2O_4^{2-}$, a marker for aged and
368 oxidized organic aerosol), sulfates, and levoglucosan (a marker for biomass burning) measurements
369 from filter samples. Table 2 summarizes the R^2 values between key tracer species and the resolved
370 aerosol factors. The two main factors resolved, in terms of mass concentration, were the OOA factors
371 with opposite diurnal trends, MO-OA and LO-OA. The concentration of MO-OA rose as the aerosol
372 number-weighted geometric mode diameter rose, also indicative of increasing aerosol age/coagulation.
373 The LO-OA factor resembled the SV-OOA factor reported by Docherty et al. (2008) measured during
374 the Study of Organic Aerosols (SOAR) project at Riverside, CA, which was also found to decrease
375 during the afternoon as temperature and photochemical processing increased. The chemical differences
376 between these two spectra are show in Figure S10 and described in the Supplementary Information.

The increase in MO-OA concentration occurred as both PTR-ToF-MS isoprene signal was increasing (also a temperature-related process) and as the 9-carbon aromatic: benzene ($C_9H_{13}^+$:$C_6H_7^+$) VOC ratio was at its minimum (related to photochemical age of air mass, (Parrish et al., 2007) . Thus, the increase MO-OA could be linked to photochemical aging of vehicular emissions during the day and/or to increasing biogenic VOC emissions and their subsequent photochemical aging and condensation into aerosol form.

The BBOA factor was found to correlate with levoglucosan (R^2=0.65, n=38); while significant levels of biomass burning from wood-burning stoves and other combustion-related heating are known to affect the Grenoble Valley in winter, such a large contribution during this season is surprising. Likely the PMF-resolved BBOA factor was somewhat mixed with emissions with close spectral signature (vehicular emissions or potentially cooking aerosol emissions). Episodic local yard-waste burning could also have contributed to the bulk aerosol spectrum, as spikes in the BBOA concentration do not appear to correlate with a particular wind direction (Figure S9). The ratio of levoglucosan: BBOA is quite low (0.03); however, it is within the order of magnitude of previously reported measurements (e.g., 0.06, (Aiken et al., 2009)). Additionally, the higher levels of oxidants found in the atmosphere in the summer could cause a faster degradation of levoglucosan in the atmosphere after emission (Hennigan et al., 2010). Thus, the BBOA concentrations reported here shall be considered as an upper limit of the biomass burning contribution.

Oxalate and OOA-Reg covaried with an R^2 of 0.62 (n=53). Regional OOA was identified as thus due to its low temporal variation, its correlation with SO_4, and a low correlation with wind direction (Figure S8). This factor was removed from the atmosphere during periods of rain and experienced a slow recovery afterwards. At the beginning of the experiment (Sept 11^{th}-13^{th}), regional OOA and SO_4 did not correspond; however, during the middle and end of the campaign, temporal variations of the regional OOA and SO_4 corresponded fairly well (R^2=0.65, n= 3328). The reason for the initial high SO_4 and low regional OOA is unclear from the data set as-is; however, MO-OA and

402 SO_4 also had similar time series trends (R^2=0.50, n=3328) and MO-OA was high at the beginning of
403 the campaign. The closeness of the two spectra's composition, as well as the nature of the aerosol type
404 (not from a specific source but rather aged bulk organic aerosol), in which variations would logically
405 occur, may have led to the imprecise separation of these two factor types.
406 Of the factors resolved, the HOA factor had the lowest O: C ratio (0.07) and a good (R^2=0.58,
407 n=3928) correlation with BC concentration. The mass spectrum of the resolved HOA factor highly
408 resembled (R^2>0.95, n=100) previously resolved HOA factors and direct AMS measurements of diesel
409 and gasoline emissions (Mohr et al., 2009; Zhang et al., 2005). HOA was not the largest average
410 contributor to the bulk measured aerosol mass over the campaign period, despite the fact that these
411 measurements were conducted 15 m from a major highway. The relative size of each type of particle
412 (primary, or HOA, and OOA) likely played a major role in the relative mass concentrations of each
413 factor (Figure S11 and discussion), and the higher increase above background of particle number
414 versus particle mass found in this study agrees with previous studies (Karner et al., 2010, Sun et al.,
415 2010). The variability of each factor over the campaign was high as, unlike measurements in more
416 rural areas, the proximity to a primary aerosol source (highway) and to an urban center (Grenoble), as
417 well as large green spaces (the Alps) allowed the full range of aged and locally transported aerosol to
418 be observed at this station.
419 *3.3.1 Fossil and Modern Carbon*
420 A source of uncertainty in the global particulate emissions of vehicles is the formation of SOA
421 from gas-phase emissions and the aging of POA. To discriminate between the relative concentration of
422 modern and fossil carbon, and thus potentially discriminate between OOA from vehicular sources and
423 from modern sources, daily filter samples were collected at the sampling site and 14C radiocarbon
424 measurements were performed. From these measurements, the percentage of modern carbon from TC
425 (OC+EC) was calculated. Modern carbon varied from 15-36% of the total aerosol carbon, a significant
426 portion of the measured carbon considering the close proximity of the measurements to fossil carbon

427 sources. In France, the contribution of biofuel was about 7% and 5% for diesel and gasoline fuel,
428 respectively, in 2011 (UFIP, Union Française des Industries Petrolières, 2011) and cannot explain this
429 relative high proportion of modern carbon observed in the particulate matter. This is similar to findings
430 shown in Hodzic et al. (2010), Minguillon et al. (2011), and El Haddad et al. (2013), which indicate
431 that modern carbon is often a significant portion of the carbonaceous fraction of PM, even in cities with
432 high vehicular emissions (e.g., Mexico City, Barcelona or Marseille).

433 As radiocarbon measurements have been performed through a thermal approach (combustion of
434 the samples at 850°C), we consider in the following section EC measured by the thermo-optical
435 method. As shown in figure S12, EC and BC agree well at low mass loadings, but have a wider scatter
436 in the data at higher mass loadings. The calculation of BC (measured by the MAAP) using an
437 absorption cross-section is imprecise and, at high loadings of BC, may under or overestimate this mass
438 loading. Figure S12 shows a comparison between the MAAP (BC) and thermal measurement (EC)
439 data, with a 1:1 line. As the thermal-optical analysis of EC is a more direct analysis, EC was chosen to
440 be used in this calculation.

441

442 Assuming that the majority of EC was traffic-related, and thus from fossil origin, the
443 concentration of modern organic carbon and fossil organic carbon was then calculated. While evidence
444 for the presence of biomass burning aerosol was measured at the field site, the main source of EC was
445 likely diesel exhaust. Figure 8 shows the fraction of EC and OC, HOA, and a partitioning between
446 fossil and modern carbon. In Figure 8A, a rough calculation was performed to determine the
447 concentration of non-primary fossil organic carbon. For a first estimate, all EC was assumed to be
448 fossil in origin. Additionally, the HOA aerosol was also assumed to be vehicular, and thus fossil, in
449 origin. The HOA factor concentration has been divided by its OM: OC ratio to remove any non-carbon
450 mass (HOA C, calculated from the elemental formulas of the PMF factor mass spectra, Aiken et al.
451 (2008)). Both EC and HOA C had high (R^2=0.89 and 0.85 respectively, n=10) correlations with the

452 fossil C mass, which supported a largely fossil source for these two species. The remaining fossil
453 organic carbon mass after subtraction was then assumed to be from non-primary sources (in light blue).
454 This calculation provided a lower estimate of the amount of fossil carbon contributing to SOA
455 mass, and involves several assumptions and potential sources of error. Sources of error in this
456 calculation include error in the PMF resolution of primary (HOA) organic aerosol spectra and error in
457 the calculated OM:OC ratio of this factor species, biodiesel vehicular emissions contributing modern
458 carbon to measured HOA, and biomass burning aerosol contributing modern carbon to measured EC.
459 As the measured HOA:EC ratio was in-line with previous measurements in high diesel environments,
460 HOA concentrations did not appear to be significantly over or under estimated. Up to 7% of fuel use in
461 France was biodiesel, thus, part of the HOA concentration could be from modern sources. While
462 research has shown that the use of biodiesel fuels reduces the overall primary particulate matter
463 emissions (Cheung et al, 2010), biodiesel could still be a modern carbon contributor to OC and EC
464 mass. Additionally, although the concentration of BBOA was generally low (a campaign average of
465 0.34 ± 0.23 $\mu g\ m^{-3}$) and the ratio of BBOA:EC has been found to be on the order of 3-4 in other areas
466 of France (Crippa et al., 2013), some contribution to EC from biomass burning may have been present
467 at the measurement site. In Figure 8B, a range of fossil non-primary organic carbon, normalized to
468 total measured organic carbon, is presented. For the upper limit of this range, HOA C and EC were
469 considered to be 95% fossil and 5% modern (7% biodiesel fuel use and an estimated 25% reduction in
470 particulate emissions from biodiesel fuel). Also for this upper limit, the calculated concentration of
471 BBOA was divided by 3 and used to calculate possible modern EC from biomass burning (Crippa et al.,
472 2013).
473 Total organic carbon concentration appeared to be more driven by processed/aged OOA
474 concentrations than by primary emissions. During the period with the highest organic concentrations
475 (September 15^{th}-17^{th}), most of the non-HOA carbon measured was modern carbon. Also during this
476 time period, the winds were also slightly more southerly and SO_4 and OOA concentrations increased,

477 which could indicate a more regional contribution to the measured air mass during this time. After a
478 period of heavy rain on the 19th, almost none of the non-HOA, organic carbon was fossil; however, this
479 also coincided with a period of increased BBOA, which may have contributed to modern-EC emissions
480 and thus an underestimate of fossil-OC emissions (Figure 7). At other times during the campaign,
481 HOA concentrations alone could not adequately explain all of the measured fossil organic carbon and
482 additional sources of fossil organic carbon (such as photochemical reactions forming aerosol from
483 vehicular VOC emissions) would be needed. Additionally, the origin of the NOA factor factor remains
484 unclear, and if fossil in origin, could explain part of the non-HOA organic fossil carbon measured at
485 the site, further reducing the OOA fossil-C (at times to almost zero). Overall, throughout the campaign
486 the majority of OOA observed was most probably modern in origin.
487 The high levels of modern carbon OOA suggested that biogenic compounds had a large effect
488 on the overall aerosol population in this location, even directly adjacent to a large anthropogenic
489 emission source (i.e., traffic). Interaction between anthropogenic oxidants and biogenic VOCs (or
490 BVOCs) has been found to increase the formation of SOA (Chameides et al., 1988; Goldstein et al.,
491 2009; Shilling et al., 2013), isoprene oxidation reactions leading towards SOA have been shown to vary
492 depending on the level of NOx (Chen et al., 2014; Kroll et al., 2005; Ng et al., 2007; Xu et al., 2014),
493 and likely BVOC concentrations were greater and the aromatic VOC concentrations were lower in the
494 wider Grenoble Valley.
495 *3.4.3. Differences between diesel-heavy and gasoline-heavy near-roadway measurements*
496 Older diesel vehicles have been shown to emit both higher levels of PM, particularly BC, and
497 higher levels of NOx. Indeed, high concentrations of NOx were measured at the field site, up to 450
498 ppbv ($NO+NO_2$) for 15 min averaged measurements. NO_2 levels exceeded the 100 ppbv European
499 hourly limit almost every morning. The campaign average for NO_2 was 94 +/- 64 ppbv. For
500 comparison, at a measurement site adjacent to a major highway in New York, Sun et al. (2012)
501 measured an average of 48 +/- 30 ppbv NO_2, about half that of this campaign's average, with 15 min

502 average peaks ranging from 100-300 ppbv. The hourly traffic concentrations at each site were close
503 (approximately 10,000 vehicles/hour reported during the Sun et al. (2012) measurement periods
504 compared to approximately 8,000 vehicles/hour observed during daylight driving hours on Grenoble's
505 highway); thus, increased NOx cannot be explained by increased traffic. Rather, increased diesel fuel
506 use is a very likely hypothesis.

507 High levels of BC were also measured in this work. A comparison of the HOA: BC ratio from
508 this study and from previously reported field studies is shown in Figure 9A. As expected, since the
509 French fleet includes a much higher percentage of diesel car with increased BC emissions, this ratio
510 was significantly lower than that reported for an urban-downwind site in Pittsburgh (1.41, Zhang et al.
511 (2005)), a highway adjacent site in New York (1.02, Sun et al. (2012)), an urban/highway site in
512 Ontario (0.7-1.1, Stroud et al. (2012)), a rural site in NW England (1.61-1.91, Liu et al. (2006)), and an
513 urban site in Zürich, Switzerland (1.1, Lanz et al. (2007)). As for measurements in France, a study in an
514 urban site in Paris observed a HOA:BC ratio of 0.61 (Crippa et al., 2013); this site was most probably
515 influenced by a vehicle fleet similar to Grenoble's, but measurements were collected during winter
516 (lower temperatures) and within Paris (increased urban emissions). Tailpipe measurements of Euro 4
517 diesel and gasoline-powered vehicles (a Renault Kangoo and a Ford Ka, respectively) at IFSTTAR
518 (Institut Français des Sciences et Technologies des Transports, de l'Aménagement et des Réseaux)
519 performed during this PM Drive research program also show a much higher HOA: BC ratio for
520 gasoline vehicles versus diesel vehicles (unpublished data). This was due to much higher BC
521 emissions from the diesel vehicle, as opposed to higher HOA emissions from the gasoline vehicle.
522 Similarly, the HOA factor measured near Grenoble was similar to that measured by Sun et al. (2012),
523 in a high gasoline environment next to a highway in New York, both in absolute concentration and
524 chemical composition; thus, an increase in BC emissions (from diesel) rather than a reduction in HOA:
525 vehicle number was likely the cause of our low HOA: BC ratio.

526 The change in HOA: BC ratio as a function of the diesel: gasoline fuel use (Road sector, World

527 Bank, 2011) is shown in Figure 9B. A decrease in HOA: BC with an increase in percent diesel is
528 clearly observable with a strong correlation (R^2=0.85, n=10), despite the many different factors
529 possibly influencing BC and HOA concentrations at each location (e.g., local aerosol sources,
530 meteorology). Such a linear relationship between HOA: BC and diesel percentage is very interesting,
531 but was not necessarily expected, since the emission factors of HOA+BC differ significantly between
532 diesel and gasoline cars, especially for pre EURO5 vehicles.

533 Additionally, an AMS factor with a diurnal pattern peaking during rush hour and with N-
534 containing peaks was observed. Saarikoski et al., (2012) found a similar amine-containing NOA factor
535 in measurements taken in the Po Valley (Italy) that also had a strong diurnal pattern. However, their
536 NOA factor was attributed to marine influence due to a correlation with MSA (Saarikoski et al., 2012),
537 although it is possible that MSA was from the local industrial use of DMSO as a solvent, and had a
538 higher H:C ratio (1.91) than the factor resolved from this data set (1.38). Like France, Italy has a large
539 percentage of diesel fuel consumption (71%, World Bank 2011). Aiken et al., (2009) and Sun et al.,
540 (2011) also resolved N-containing OA factors from data measured in Mexico City and New York,
541 respectively, but did not observe a similar diurnal pattern. In the PTR-ToF-MS mass spectra results
542 obtained from Euro 5 vehicle emission smog chamber studies, Hellebust et al., (2015 and 2013) found
543 higher nitrogen-containing emissions from fresh and aged diesel mass than from fresh and aged
544 gasoline mass spectra (e.g., peaks such as $CH_4NO_2^+$). Similar nitrogen-containing VOC peaks were
545 found by Inomata et al. (2013) in diesel exhaust. Thus, diesel-related emissions could possibly be the
546 source for the observed NOA factor, although no significant correlation between this factor and other
547 vehicular emissions, such as BC, was found. More detail on the NOA factor can be found in the
548 Supplementary Information and Figure S13.

549 And finally, only small amounts OOA measured at the field site were calculated to contain
550 fossil-OC. Work by Bahreini et al., (2010) found that much of the measured SOA in the Los Angeles
551 Valley was from gasoline passenger cars, not from diesel trucks, and perhaps the relatively low

552 concentration of gasoline vehicles on the road in France is related to the low concentration of fossil-
553 OOA.
554
555 **4. Conclusions**
556 During this campaign, highly time resolved particle and gas-phase chemical composition and
557 concentration measurements were obtained alongside parallel traffic data of the speed, fluxes, vehicle
558 type, and fuel type of passing cars on a highway in the Grenoble Valley. An analysis of the local
559 primary (traffic) aerosol and the more regional, aged secondary organic aerosol was performed for the
560 PM1 fraction observed by the HR-ToF-AMS. The PMF model was run on the high-resolution HR-
561 ToF-AMS aerosol data and six factors were resolved from the bulk aerosol data: 1) an HOA factor,
562 related to traffic 2) a BBOA factor 3) a regional OOA factor, which covaried with sulfate 4) a MO-OA
563 factor, increasing in concentration during sunny afternoons 5) a LO-OA factor, with the opposite
564 diurnal pattern as MO-OA, likely due to gas-particle phase partitioning and photochemical processing
565 and 6) an NOA factor with a diurnal pattern similar to that of HOA and to traffic peaks.
566 The resolved mass spectrum for the HOA factor was chemically similar to mass spectra from
567 both gasoline and diesel-emitted organic carbon and previously resolved HOA factors in high-gasoline
568 environments; however, the HOA: BC ratio measured was low (<0.3) throughout the campaign. This
569 ratio agrees with previously reported HOA: BC ratios in high diesel environments and from direct
570 measurements of diesel emissions in smog chamber and tailpipe measurement studies. The fraction of
571 diesel-powered vehicles on the road appeared to control, to some extent, this ratio. Diesel also
572 influenced local NOx concentrations, as the measured NOx was two times higher than concentrations
573 near a similarly-trafficked highway in New York, USA.
574 While high levels of both black carbon (5 +/- 3 $\mu g\ m^{-3}$) and organic aerosol (8 +/- 4 $\mu g\ m^{-3}$)
575 were measured, when examined, only 20% of the total organic mass signal could be attributed to
576 primary vehicular emissions (i.e., HOA). Significant amounts of modern organic carbon were also

measured, and fossil carbon appeared to contribute only a small amount to the measured OOA. Although NOx and VOCs emitted by diesel and gasoline engines, respectively, may have influenced SOA formation in the Grenoble Valley, the majority of OOA measured was modern in origin, even adjacent to a major source of fossil carbon. Whether this is due to a lower overall gas+particle emission of diesel vehicles, the lack of aromatic compounds in diesel VOC emissions, high NOx reducing the efficiency of vehicular VOC to SOA formation mechanisms, an acceleration of BVOC to biogenic aerosol formation in the presence of vehicular emissions, or simply the more global source and higher efficiency of BVOC to SOA reactions is unclear, but in a high diesel environment, SOA OOA from fossil-fuel carbon was only a small source of the measured OOA , while modern C-containing OOA dominated the organic aerosol mass in the fine fraction of PM1.

Acknowledgments:

This work was supported by the French Environment and Energy Management Agency (ADEME, Grant number 1162C0002). The authors gratefully acknowledge the NOAA Air Resources Laboratory (ARL) for the provision of the HYSPLIT transport and dispersion model (http://www.ready.noaa.gov) used in this publication. We also gratefully acknowledge Air Rhone Alpes staff (particularly Yann Pellan) for their support during the campaign as well as Y. Sun and Q. Zhang for providing near-highway aerosol data from their paper Sun et al., (2012) for comparison with these measurement, and the MASSALYA instrumental platform (Aix Marseille Université, lce.univ-amu.fr) for the analysis and measurements used in this publication. Finally, the authors would like to acknowledge and thank the two anonymous reviewers who provided constructive advice on the formation of the final paper.

602

603

604

605

606

607

608
609

610

611 Table 1

612

PMF FACTOR	OM:OC	H:C	O:C
HOA	1.25	1.89	0.07
NOA	1.69	1.38	0.4
LO-OA	1.74	1.34	0.47
MO-OA	2.15	1.16	0.78
BBOA	1.56	1.47	0.32
OOA-REG	1.85	1.54	0.52

613

614

615

616

617

618

619

620

621

622

623

624

PMF FACTOR	Oxalate (N=53) R^2	BC[a] (N=3928) R^2	Levoglucosan (N=38) R^2	Sulfate (N=3328)[b] R^2
HOA	0.01	0.58	0.12	0.004
BBOA	0.04	0.05	0.65	0.005
MO-OA	0.50	0.01	0.02	0.54
LO-OA	0.32	0.01	0.08	0.07
NOA	0.01	0.09	0.12	0.06
OOA-REG	0.62	0.02	0.01	0.65

[a.] BC data smoothed to remove underestimated BC concentrations during periods of high filter loading (Hyvärinen et al., 2013)

[b.] R^2 value calculated after initial high SO_4 period.

Figure Captions

Figure 1: The measurement site location is marked by a red square on the map, and the adjacent highway has been colored in red. A detailed view of the measurement site and the two measurement stations is shown in the lower right-hand corner in the upper right-hand corner is the wind rose and polar plots for black carbon and NO, with the red lines denoting the direction of the highway. Grenoble is to the north.

Figure 2: The non-refractory submicrometer aerosol concentration in μg m^{-3} of SO_4, NH_4, NO_3, and Organic species is plotted along with black carbon for the campaign time series. (A), 15 minute traffic concentration (missing data due to malfunction in the traffic cameras on those days) (B) COO^+ (*m/z* 44) and $C_4H_9^+$ (*m/z* 57) (C), and the number-weighted geometric size distribution (D) with the total number concentration of particles as a function of time (D, right axis). The inset (a-1) shows average concentrations of the species in a) for high traffic and all traffic periods. The color legend is the same for a and a-1.

Figure 3: The concentration in ppbv of PTR-ToF-MS VOC species identified isoprene and MVK/Methacrolin (left axis, A), VOC species associated with diesel exhaust ($CH_4NO_2^+$, $C_2H_5O^+$, B),VOC species associated with gasoline exhaust ($C_6H_7^+$, C_9H13^+, C). NO and NO_2 (gas-phase) ppbv concentrations (D) and ambient temperature (right axis, A) during the measurement period are also shown.

Figure 4: Diurnal profiles of boundary-layer scaled VOC peaks from PTR-ToF-MS measurements and BC peaks from MAAP measurements (A), temperature (right axis, B), boundary layer height (left axis, B), vehicular speed (left axis, C) and vehicle concentration (right axis, C).

Figure 5: The mass spectra of the six resolved factors, more oxidized organic aerosol (MO-OA), less oxidized organic aerosol (LO-OA), regional oxidized organic aerosol (reg-OOA), biomass burning organic aerosol (BBOA), hydrocarbon-like organic aerosol (HOA), and nitrogen-containing organic aerosol (NOA). Fraction of total signal is plotted against *m/z* and the peaks are color-coded to show their high-resolution identifications.

Figure 6: The diurnal profiles (A) and concentration and standard deviation of the six resolved aerosol factors (B).

Figure 7: The time series of the six-factor PMF solution (A), the resolved BBOA factor time series concentration (right axis, B) and off-line levoglucosan measurements (left axis, B), the resolved HOA factor time series concentration and BC (right axis, C), HR-TOF-AMS-measured SO_4 and the resolved regional OOA factor (left axis, D) and off-line oxalate measurements (right axis, right). The inset (a-1) shows the calculated mass contribution during all (left) and high traffic (right) periods of each resolved PMF factor (same color legend for a and a-1).

Figure 8: Measured EC and OC, with calculated contribution of non-primary fossil organic carbon (assuming 100% fossil EC and HOA, A) and assuming partial modern organic carbon EC and HOA contribution (B). The possible fossil OOA (light blue) was calculated by the subtraction of HOA from the fossil-OC fraction (assuming HOA either all fossil, A, or 95% fossil, B, and EC either all fossil (a) or 5%+BBOA/3 modern (b).

Figure 9:
Calculated HOA and measured BC concentrations from the campaign and HOA: BC ratios from previous field campaigns. Grey area is shaded to include a diesel-only environment and two French HOA: BC ratios: one from Crippa et al., (2013) and from this study (A). The HOA: BC ratio from various literature sources versus percent diesel fuel use out of total fuel use for the country of study (B).

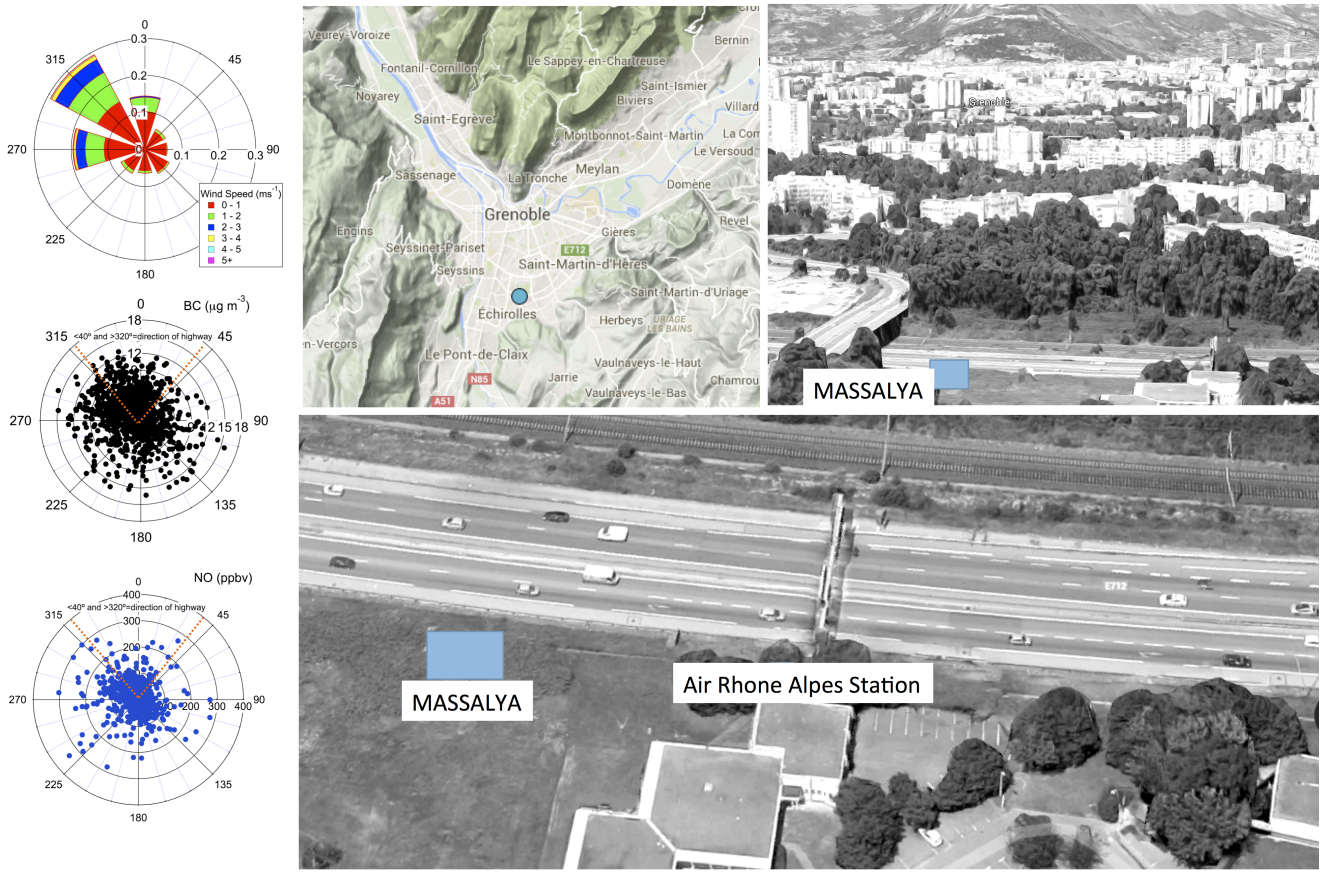

Figure 1

The measurement site location is marked by a red square on the map, and the adjacent highway has been colored in red. A detailed view of the measurement site and the two measurement stations is shown in the lower right-hand corner in the upper right-hand corner is the wind rose and polar plots for black carbon and NO, with the red lines denoting the direction of the highway. Grenoble is to the north.

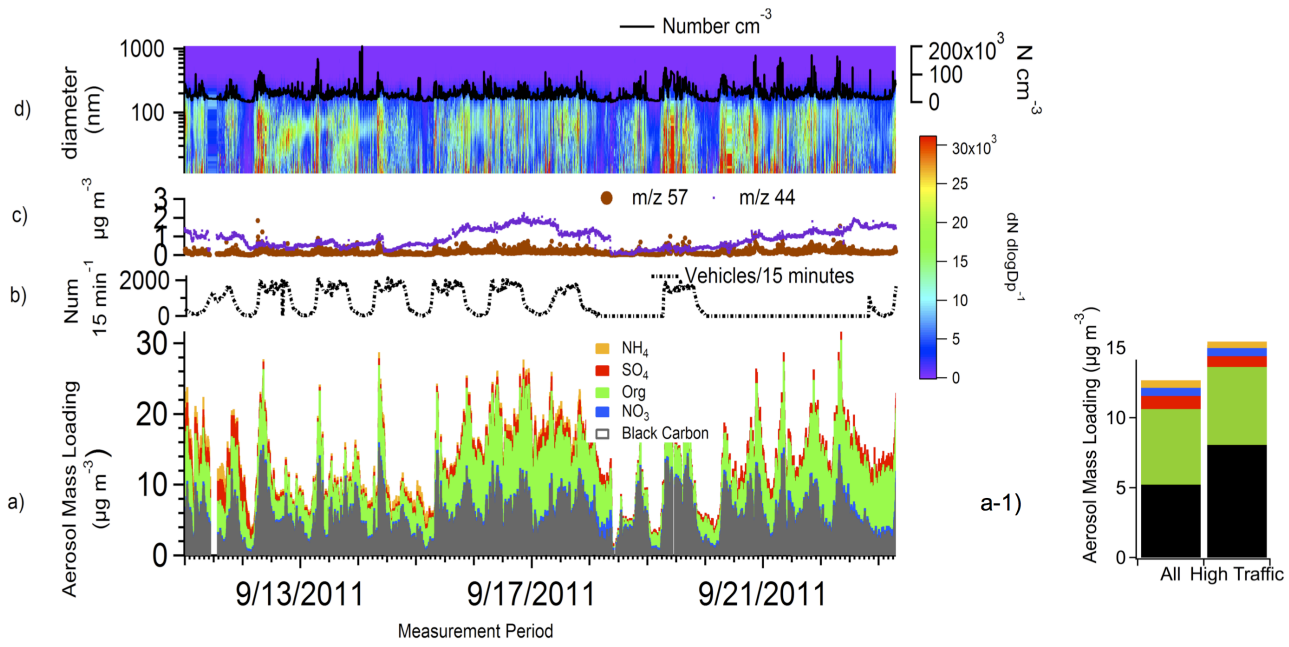

Figure 2: The non-refractory submicrometer aerosol concentration in μg m^{-3} of SO_4, NH_4, NO_3, and Organic species is plotted along with black carbon for the campaign time series. (A), 15 minute traffic concentration (missing data due to malfunction in the traffic cameras on those days) (B) COO^+ (*m/z* 44) and $C_4H_9^+$ (*m/z* 57) (C), and the number-weighted geometric size distribution (D) with the total number concentration of particles as a function of time (D, right axis). The inset (a-1) shows average concentrations of the species in a) for high traffic and all traffic periods. The color legend is the same for a and a-1.

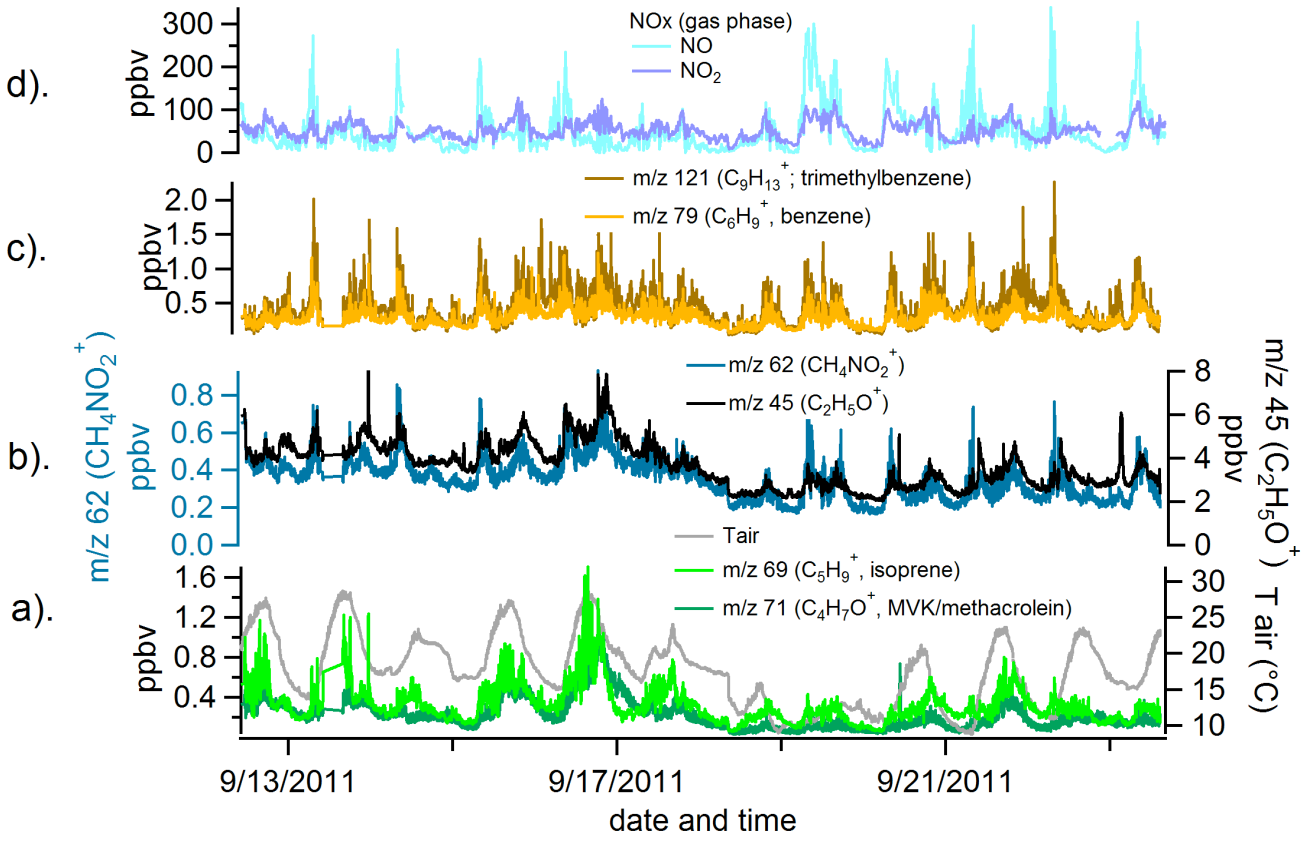

Figure 3
The concentration in ppbv of PTR-ToF-MS VOC species identified isoprene and MVK/Methacrolin (left axis, A), VOC species associated with diesel exhaust ($CH_4NO_2^+$, $C_2H_5O^+$, B),VOC species associated with gasoline exhaust ($C_6H_7^+$, C_9H13^+, C). NO and NO_2 (gas-phase) ppbv concentrations (D) and ambient temperature (right axis, A) during the measurement period are also shown.

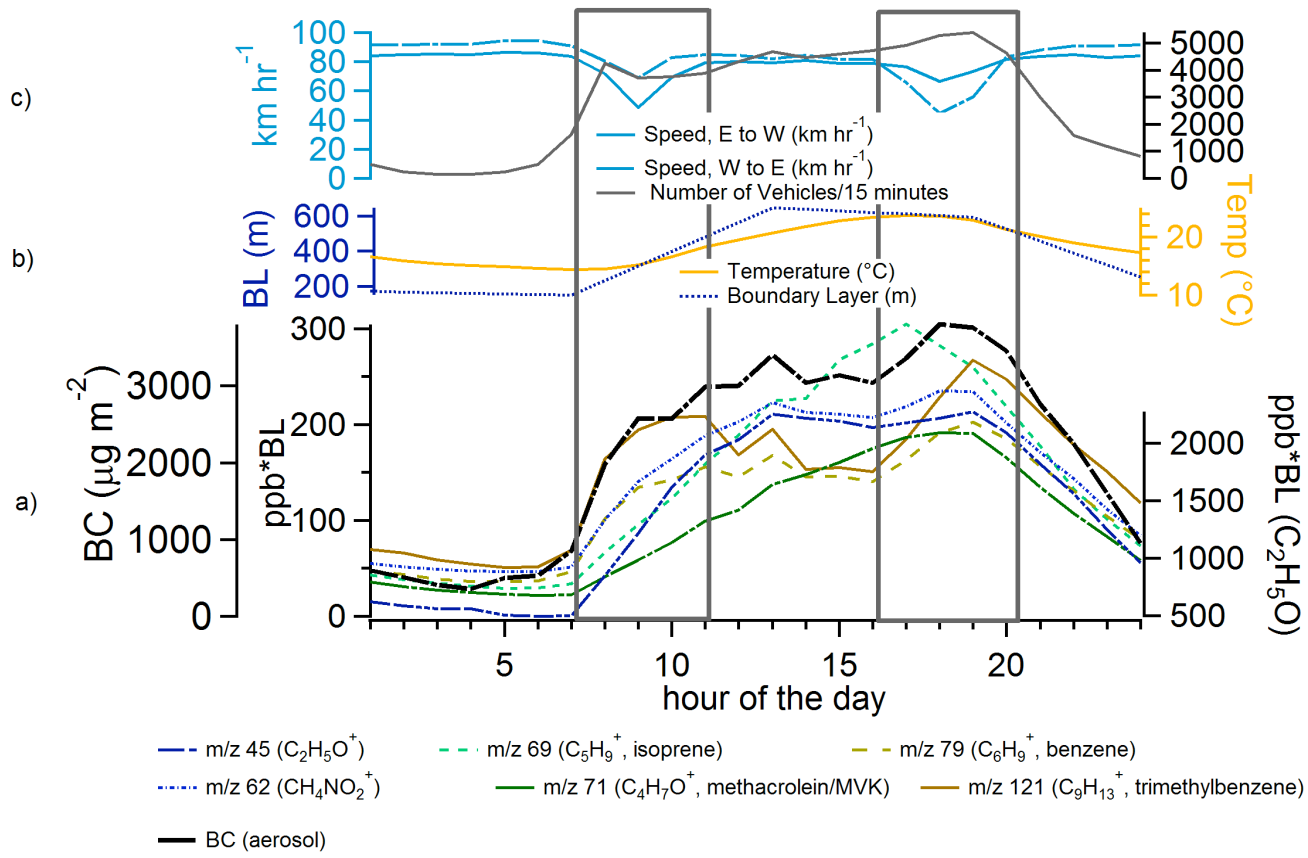

Figure 4 Diurnal profiles of boundary-layer scaled VOC peaks from PTR-MS measurements and BC peaks from MAAP measurements (A), temperature (right axis, B), boundary layer height (left axis, B), vehicular speed (left axis, C) and vehicle concentration (right axis, C).

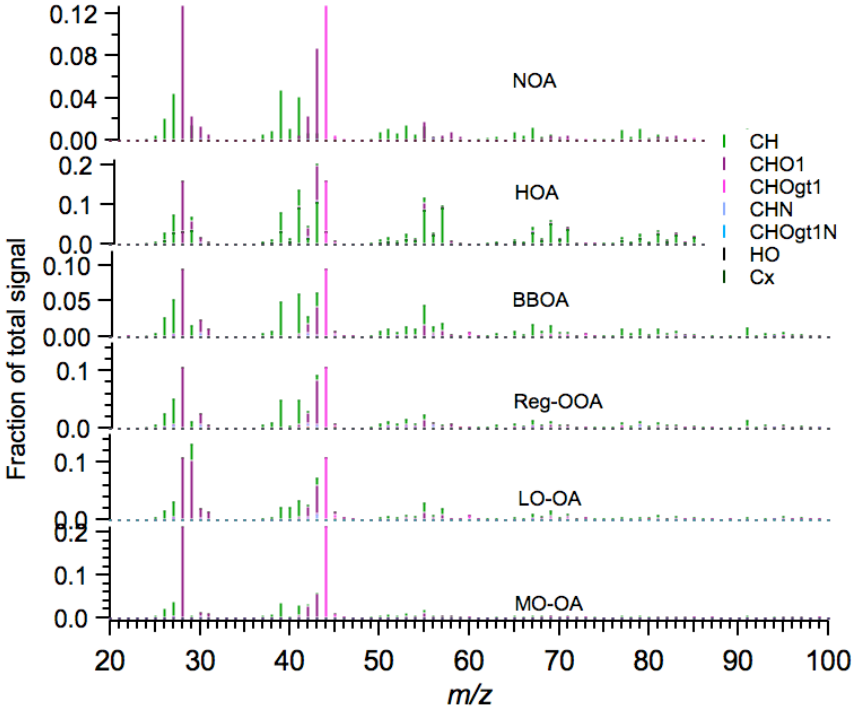

Figure 5:
The mass spectra of the six resolved factors, more oxidized organic aerosol (MO-OA), less oxidized organic aerosol (LO-OA), regional oxidized organic aerosol (reg-OOA), biomass burning organic aerosol (BBOA), hydrocarbon-like organic aerosol (HOA), and nitrogen-containing organic aerosol (NOA). Fraction of total signal is plotted against *m/z* and the peaks are color-coded to show their high-resolution identifications.

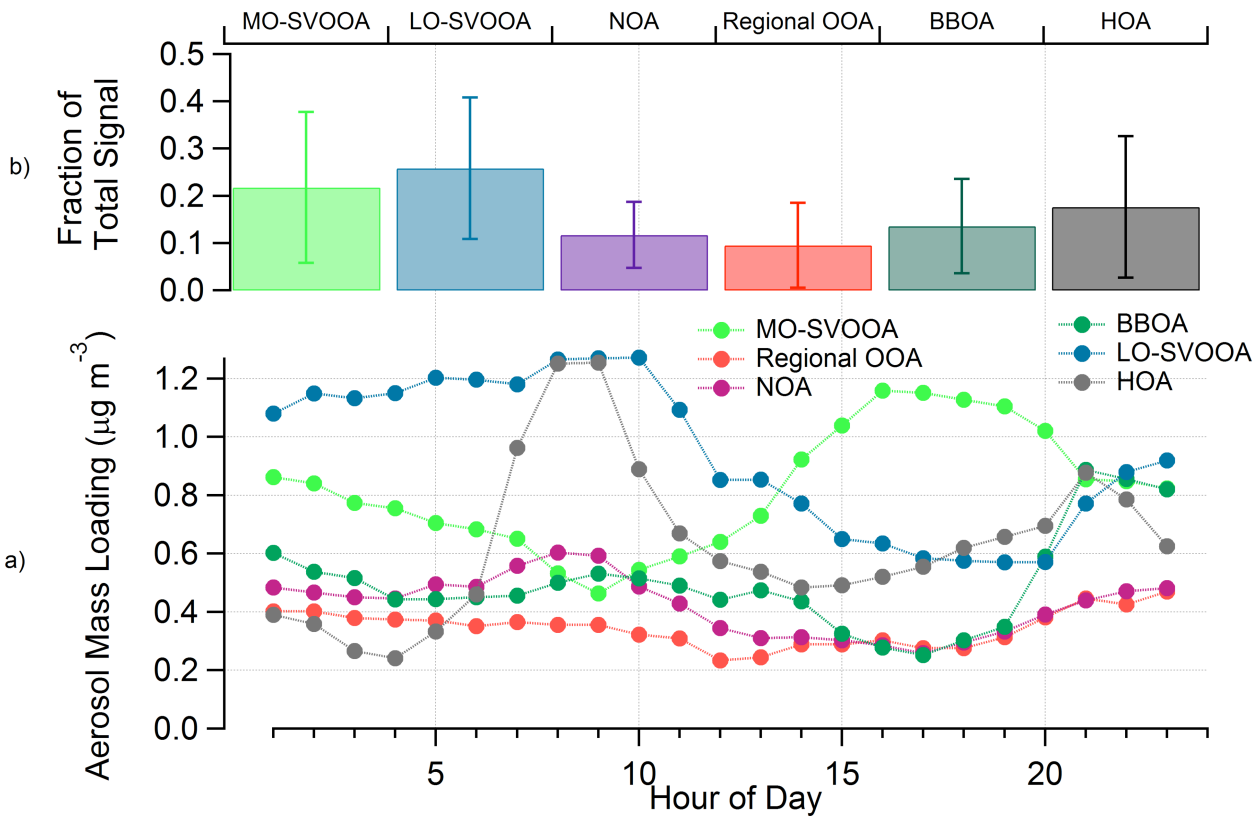

Figure 6: The diurnal profiles (A) and concentration and standard deviation of the six resolved aerosol factors (B).

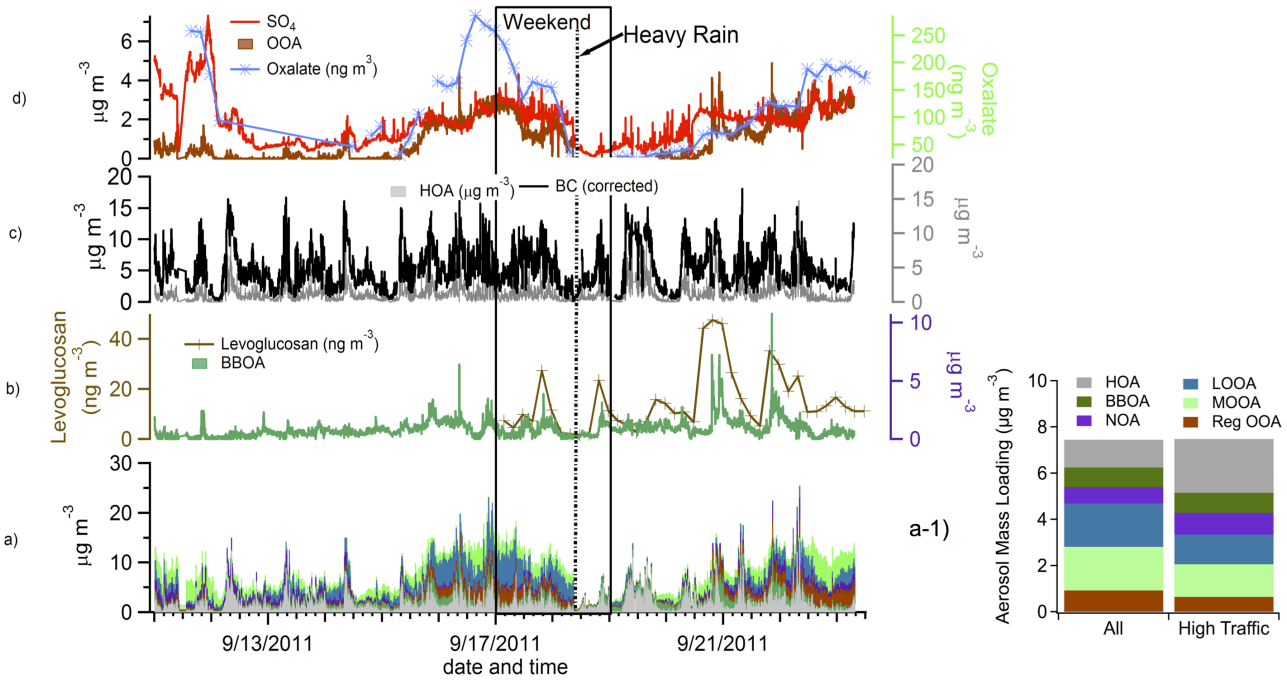

Figure 7:

The time series of the six-factor PMF solution (A), the resolved BBOA factor time series concentration (right axis, B) and off-line levoglucosan measurements (left axis, B), the resolved HOA factor time series concentration and BC (right axis, C), HR-TOF-AMS-measured SO_4 and the resolved regional OOA factor (left axis, D) and off-line oxalate measurements (right axis, right). The inset (a-1) shows the calculated mass contribution during all (left) and high traffic (right) periods of each resolved PMF factor (same color legend for a and a-1).

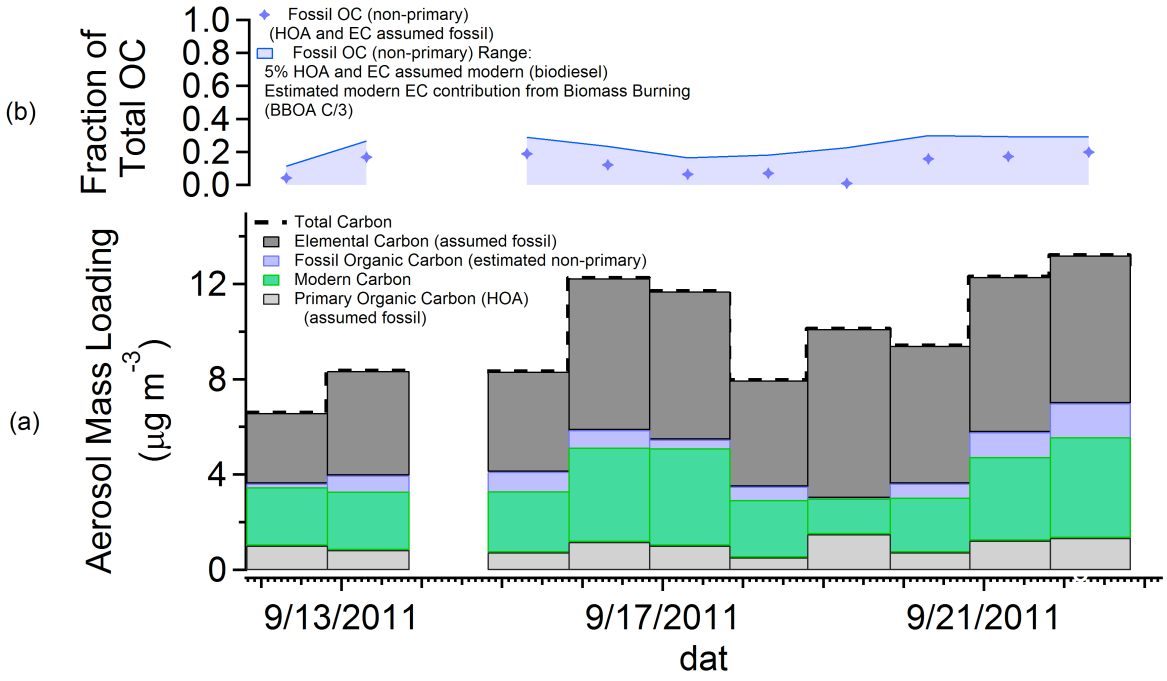

Figure 8: Measured EC and OC, with calculated contribution of non-primary fossil organic carbon (assuming 100% fossil EC and HOA, a) and assuming partial modern organic carbon EC and HOA contribution (b). The possible fossil OOA (light blue) was calculated by the subtraction of HOA from the fossil-OC fraction (assuming HOA either all fossil, A, or 95% fossil, B, and EC either all fossil (a) or 5%+BBOA/3 modern (b).

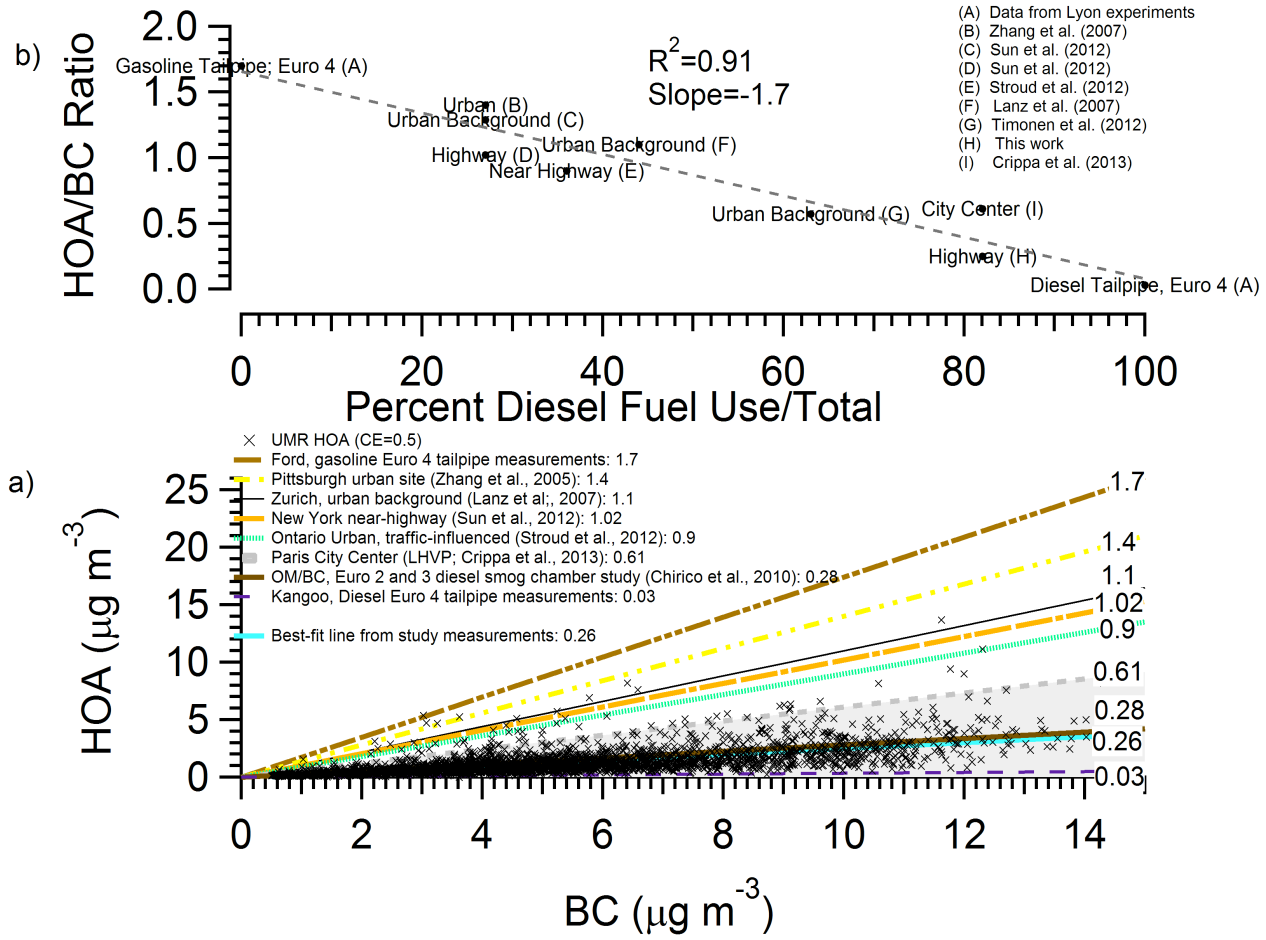

892 Figure 9
893 Calculated HOA and measured BC concentrations from the campaign and HOA: BC ratios from
894 previous field campaigns. Grey area is shaded to include a diesel-only environment and two French
895 HOA: BC ratios: one from Crippa et al., (2013) and from this study (A). The HOA: BC ratio from
896 various literature sources versus percent diesel fuel use out of total fuel use for the country of study (B).
897
898
899
900
901
902
903
904
905
906
907
908
909

References

Aiken, A. C., Salcedo, D., Cubison, M. J., Huffman, J. a., DeCarlo, P. F., Ulbrich, I. M., Docherty, K. S., Sueper, D., Kimmel, J. R., Worsnop, D. R., Trimborn, a., Northway, M., Stone, E. a., Schauer, J. J., Volkamer, R., Fortner, E., de Foy, B., Wang, J., Laskin, a., Shutthanandan, V., Zheng, J., Zhang, R., Gaffney, J., Marley, N. a., Paredes-Miranda, G., Arnott, W. P., Molina, L. T., Sosa, G. and Jimenez, J. L.: Mexico City aerosol analysis during MILAGRO using high resolution aerosol mass spectrometry at the urban supersite (T0) – Part 1: Fine particle composition and organic source apportionment, Atmos. Chem. Phys., 9(2), 8377–8427, doi:10.5194/acpd-9-8377-2009, 2009.

Aiken, A. C., Decarlo, P. F., Kroll, J. H., Worsnop, D. R., Huffman, J. A., Docherty, K. S., Ulbrich, I. M., Mohr, C., Kimmel, J. R., Sueper, D., Sun, Y., Zhang, Q., Trimborn, A., Northway, M., Ziemann, P. J., Canagaratna, M. R., Onasch, T. B., Alfarra, M. R., Prevot, A. S. H., Dommen, J., Duplissy, J., Metzger, A., Baltensperger, U. and Jimenez, J. L.: O/C and OM/OC ratios of primary, secondary, and ambient organic aerosols with high-resolution time-of-flight aerosol mass spectrometry., Environ. Sci. Technol., 42(12), 4478–85.

Bahreini, R., Middlebrook, a. M., de Gouw, J. a., Warneke, C., Trainer, M., Brock, C. a., Stark, H., Brown, S. S., Dube, W. P., Gilman, J. B., Hall, K., Holloway, J. S., Kuster, W. C., Perring, a. E., Prevot, a. S. H., Schwarz, J. P., Spackman, J. R., Szidat, S., Wagner, N. L., Weber, R. J., Zotter, P. and Parrish, D. D.: Gasoline emissions dominate over diesel in formation of secondary organic aerosol mass, Geophys. Res. Lett., 39(6), doi:10.1029/2011GL050718, 2012.

Birch, M. E. and Cary, R. A.: Elemental Carbon-Based Method for Monitoring Occupational Exposures to Particulate Diesel Exhaust, Aerosol Sci. Technol., 25(3), 221–241, 1996.

Bond, T. C., Doherty, S. J., Fahey, D. W., Forster, P. M., Berntsen, T., DeAngelo, B. J., Flanner, M. G., Ghan, S., Kärcher, B., Koch, D., Kinne, S., Kondo, Y., Quinn, P. K., Sarofim, M. C., Schultz, M. G., Schulz, M., Venkataraman, C., Zhang, H., Zhang, S., Bellouin, N., Guttikunda, S. K., Hopke, P. K., Jacobson, M. Z., Kaiser, J. W., Klimont, Z., Lohmann, U., Schwarz, J. P., Shindell, D., Storelvmo, T., Warren, S. G. and Zender, C. S.: Bounding the role of black carbon in the climate system: A scientific assessment, J. Geophys. Res. Atmos., 118(11), 5380–5552, doi:10.1002/jgrd.50171, 2013.

Broderick, B. and Marnane, I.: A comparison of the C2–C9 hydrocarbon compositions of vehicle fuels and urban air in Dublin, Ireland, Atmos. Environ., 36(6), 975–986, doi:10.1016/S1352-2310(01)00472-1, 2002.

Brugge, D., Durant, J. L. and Rioux, C.: Near-highway pollutants in motor vehicle exhaust: a review of epidemiologic evidence of cardiac and pulmonary health risks., Environ. Health, 6, 23, doi:10.1186/1476-069X-6-23, 2007.

Bruns, E. A, Perraud, V., Zelenyuk, A., Ezell, M. J., Johnson, S. N., Yu, Y., Imre, D., Finlayson-Pitts, B. J. and Alexander, M. L.: Comparison of FTIR and particle mass spectrometry for the measurement of particulate organic nitrates., Environ. Sci. Technol., 44(3), 1056–61, doi:10.1021/es9029864, 2010.

Carlton, A. G., Wiedinmyer, C. and Kroll, J. H.: A review of Secondary Organic Aerosol (SOA) formation from isoprene, Atmos. Chem. Phys. Discuss., 9(2), 8261–8305, doi:10.5194/acpd-9-8261-2009, 2009.

Cavalli, F., Viana, M., Yttri, K. E., Genberg, J. and Putaud, J.-P.: Toward a standardised thermal-optical protocol for measuring atmospheric organic and elemental carbon: the EUSAAR protocol, Atmos. Meas. Tech., 3(1), 79–89, 2010.

950 Chameides, W., Lindsay, R., Richardson, J. and Kiang, C.: The role of biogenic hydrocarbons in urban
951 photochemical smog: Atlanta as a case study, Science (80-83)., 241(4872), 1473–1475,
952 doi:10.1126/science.3420404, 1988.

953 Chen, J., Zhao, C. S., Ma, N. and Yan, P.: Aerosol hygroscopicity parameter derived from the light scattering
954 enhancement factor measurements in the North China Plain, Atmos. Chem. Phys., 14(15), 8105–8118,
955 doi:10.5194/acp-14-8105-2014, 2014.

956 Cheung, K.L., Ntziachristos, L.,Tzamkiozis, T., Schauer, J.J., Samaras, Z., Moore, K.F. & Sioutas, C. (2010)
957 Emissions of Particulate Trace Elements, Metals and Organic Species from Gasoline, Diesel, and Biodiesel Pas-
958 senger Vehicles and Their Relation to Oxidative Potential, Aerosol Science and Technology, 44:7, 500-513,
959 DOI: 10.1080/02786821003758294

960 Chirico, R., Decarlo, P. F., Heringa, M. F., Tritscher, T., Richter, R. and Pr, A. S. H.: Impact of aftertreatment
961 devices on primary emissions and secondary organic aerosol formation potential from in-use diesel vehicles :
962 results from smog chamber experiments, Atmos. Chem. Phys., 11545–11563, doi:10.5194/acp-10-11545-2010,
963 2010.

964 Crippa, M., DeCarlo, P. F., Slowik, J. G., Mohr, C., Heringa, M. F., Chirico, R., Poulain, L., Freutel, F., Sciare,
965 J., Cozic, J., Di Marco, C. F., Elsasser, M., Nicolas, J. B., Marchand, N., Abidi, E., Wiedensohler, A., Drewnick,
966 F., Schneider, J., Borrmann, S., Nemitz, E., Zimmermann, R., Jaffrezo, J.-L., Prévôt, A. S. H. and Baltensperger,
967 U.: Wintertime aerosol chemical composition and source apportionment of the organic fraction in the
968 metropolitan area of Paris, Atmos. Chem. Phys., 13(2), 961–981, doi:10.5194/acp-13-961-2013, 2013.

969 Decarlo, P. F., Kimmel, J. R., Trimborn, A., Northway, M. J., Jayne, J. T., Aiken, A. C., Gonin, M., Fuhrer, K.,
970 Horvath, T., Docherty, K. S., Worsnop, D. R. and Jimenez, J. L.: Field-Deployable, high-resolution, time-of-
971 flight aerosol mass spectrometer, Anal. Chem., 78(24), 8281–8289, doi:8410.1029/2001JD001213. 2006.

972 Docherty, K. S., Stone, E. A., Ulbrich, I. M., DeCarlo, P. F., Snyder, D. C., Schauer, J. J., Peltier, R. E., Weber,
973 R. J., Murphy, S. M., Seinfeld, J. H., Grover, B. D., Eatough, D. J. and Jimenez, J. L.: Apportionment of Primary
974 and Secondary Organic Aerosols in Southern California during the 2005 Study of Organic Aerosols in Riverside
975 (SOAR-1), Environ. Sci. Technol., 42(20), 7655–7662, doi:10.1021/es8008166, 2008.

976 El Haddad, I., Marchand, N., Dron, J., Temime-Roussel, B., Quivet, E., Wortham, H., Jaffrezo, J. L., Baduel, C.,
977 Voisin, D., Besombes, J. L. and Gille, G.: Comprehensive primary particulate organic characterization of
978 vehicular exhaust emissions in France, Atmos. Environ., 43(39), 6190–6198,
979 doi:10.1016/j.atmosenv.2009.09.001, 2009.

980 El Haddad, I., Marchand, N., Wortham, H., Piot, C., Besombes, J.-L., Cozic, J., Chauvel, C., Armengaud, a.,
981 Robin, D. and Jaffrezo, J.-L.: Primary sources of $PM_{2.5}$ organic aerosol in an industrial Mediterranean city,
982 Marseille, Atmos. Chem. Phys., 11(5), 2039–2058, doi:10.5194/acp-11-2039-2011, 2011.

983 El Haddad, I., D'Anna, B., Temime-Roussel, B., Nicolas, M., Boreave, A., Favez, O., Voisin, D., Sciare, J.,
984 George, C., Jaffrezo, J.-L., Wortham, H., and Marchand, N.: Towards a better understanding of the origins,
985 chemical composition and aging of oxygenated organic aerosols: case study of a Mediterranean industrialized
986 environment, Marseille, Atmos. Chem. Phys., 13, 7875-7894, doi:10.5194/acp-13-7875-2013, 2013.

987 Farmer, D. K., Matsunaga, a, Docherty, K. S., Surratt, J. D., Seinfeld, J. H., Ziemann, P. J. and Jimenez, J. L.:
988 Response of an aerosol mass spectrometer to organonitrates and organosulfates and implications for atmospheric
989 chemistry., Proc. Natl. Acad. Sci. U. S. A., 107(15), 6670–5, doi:10.1073/pnas.0912340107, 2010.

990 Favez, O., El Haddad, I., Piot, C., Boréave, a., Abidi, E., Marchand, N., Jaffrezo, J.-L., Besombes, J.-L.,
991 Personnaz, M.-B., Sciare, J., Wortham, H., George, C. and D'Anna, B.: Inter-comparison of source
992 apportionment models for the estimation of wood burning aerosols during wintertime in an Alpine city
993 (Grenoble, France), Atmos. Chem. Phys., 10(12), 5295–5314, doi:10.5194/acp-10-5295-2010, 2010.

994 Fry, J. L., Draper, D. C., Zarzana, K. J., Campuzano-Jost, P., Day, D. a., Jimenez, J. L., Brown, S. S., Cohen, R.
995 C., Kaser, L., Hansel, A., Cappellin, L., Karl, T., Hodzic Roux, A., Turnipseed, A., Cantrell, C., Lefer, B. L. and
996 Grossberg, N.: Observations of gas- and aerosol-phase organic nitrates at BEACHON-RoMBAS 2011, Atmos.
997 Chem. Phys., 13(17), 8585–8605, doi:10.5194/acp-13-8585-2013, 2013.

998 Gentner, D. R., Isaacman, G., Worton, D. R., Chan, A. W. H., Dallmann, T. R., Davis, L., Liu, S., Day, D. a,
999 Russell, L. M., Wilson, K. R., Weber, R., Guha, A., Harley, R. a and Goldstein, A. H.: Elucidating secondary
1000 organic aerosol from diesel and gasoline vehicles through detailed characterization of organic carbon emissions.,
1001 Proc. Natl. Acad. Sci. U. S. A., 109(45), 18318–23, doi:10.1073/pnas.1212272109, 2012.

1002 Goldstein, A. H., Koven, C. D., Heald, C. L. and Fung, I. Y.: Biogenic carbon and anthropogenic pollutants
1003 combine to form a cooling haze over the southeastern United States, Proc. Natl. Acad. Sci., 106(22), 8835–8840,
1004 doi:10.1073/pnas.0904128106, 2009.

1005 Hellebust, S., Temime-Roussel, B., Bertrand, A., Platt, S. M., El Haddad, I., Pieber, S., Zardini, A. A., Suarez-
1006 Bertoa, R., Slowik, J. G., Huang, R. J., Astorga, C., Prevot, A. S. H. and Marchand, N.: Comparison of Gasoline
1007 and Diesel Vehicles-Emission Factors of Volatile Organic Compounds from EURO5 Diesel and Gasoline
1008 Vehicles and Their Potential Integrated Influence on Air Quality, Am. Assoc. Aerosol Res., Fall 2013 , 2013.

1009 Hellebust, S., Temime-Roussel, B., Bertrand, A., Platt, S. M., El Haddad, I., Pieber, S., Zardini, A. A., Suarez-
1010 Bertoa, R., Slowik, J. G., Huang, R. J., Astorga, C., Prevot, A. S. H. and Marchand, N.: Emission factors of Vol-
1011 atile Organic Compounds measured by Proton Transfer Reaction – Time -of-Flight – Mass Spectrometry 1. Euro
1012 2 scooter, Euro 5 light duty gasoline and diesel vehicles and Euro V heavy duty diesel vehicles (in preparation).

1013 Hennigan, C. J., Sullivan, A. P., Collett, J. L. and Robinson, A. L.: Levoglucosan stability in biomass burning
1014 particles exposed to hydroxyl radicals, Geophys. Res. Lett., 37(9), doi:10.1029/2010GL043088, 2010.

1015 Herich, H., Gianini, M. F. D., Piot, C., Močnik, G., Jaffrezo, J.-L., Besombes, J.-L., Prévôt, A. S. H. and
1016 Hueglin, C.: Overview of the impact of wood burning emissions on carbonaceous aerosols and PM in large parts
1017 of the Alpine region, Atmos. Environ., 89, 64–75, doi:10.1016/j.atmosenv.2014.02.008, 2014.

1018 Hodzic, A., Jimenez, J. L., Madronich, S., Canagaratna, M. R., DeCarlo, P. F., Kleinman, L. and Fast, J.:
1019 Modeling organic aerosols in a megacity: potential contribution of semi-volatile and intermediate volatility
1020 primary organic compounds to secondary organic aerosol formation, Atmos. Chem. Phys., 10(12), 5491–5514,
1021 doi:10.5194/acp-10-5491-2010, 2010.

1022 Huffman, J. A., Jayne, J. T., Drewnick, F., Aiken, A. C., Onasch, T., Worsnop, D. R. and Jimenez, J. L.: Design,
1023 Modeling, Optimization, and Experimental Tests of a Particle Beam Width Probe for the Aerodyne Aerosol
1024 Mass Spectrometer, Aerosol Sci. Technol., 39(12), 1143–1163, doi:10.1080/02786820500423782, 2005.

1025 Hyvärinen, A.-P., Vakkari, V., L. Laakso, R. K. Hooda, Sharma, V. P., Panwar, T. S., Beukes, J. P., van Zyl, P.
1026 G., Josipovic, M., Garland, R. M., Andreae, M. O., Pöschl, U. and Petzold, A.: Correction for a measurement
1027 artifact of the Multi-Angle Absorption Photometer (MAAP) at high black carbon mass concentration levels,
1028 Atmos. Meas. Tech., 6(1), 81–90, doi:10.5194/amt-6-81-2013, 2013.

1029 Inomata, S., Tanimoto, H., Fujitani, Y., Sekimoto, K., Sato, K., Fushimi, A., Yamada, H., Hori, S., Kumazawa,
1030 Y., Shimono, A. and Hikida, T.: On-line measurements of gaseous nitro-organic compounds in diesel vehicle

exhaust by proton-transfer-reaction mass spectrometry, Atmos. Environ., 73(x), 195–203, doi:10.1016/j.atmosenv.2013.03.035, 2013.

Jaffrezo, J. L., Davidson, C. I., Kuhns, H. D., Bergin, M. H., Hillamo, R., Maenhaut, W., Kahl, J. W. and Harris, J. M.: Biomass burning signatures in the atmosphere of central Greenland. J. Geophys. Res: Atmos., 103, 1998.

Jaffrezo, J.-L., Aymoz, G. and Cozic, J.: Size distribution of EC and OC in the aerosol of Alpine valleys during summer and winter, Atmos. Chem. Phys., 5(11), 2915–2925, 2005

Janssen, N. A. H., World Health Organization, Regional Office for Europe and Joint WHO/Convention Task Force on the Health Aspects of Air Pollution: Health effects of black carbon. [online] Available from: http://www.euro.who.int/__data/assets/pdf_file/0004/162535/e96541.pdf, 2012.

Karner, A. A., Eisinger, D. S., and Niemeier, D. A. (2010). "Near-RoadwayAir Quality: Synthesizing the Findings from Real-World Data." Environ. Sci. and Tech, 44, 5334–5344.

Kroll, J. H., Ng, N. L., Murphy, S. M., Flagan, R. C. and Seinfeld, J. H.: Secondary organic aerosol formation from isoprene photooxidation under high-NO x conditions, Geophys. Res. Lett., 32(18), doi:10.1029/2005GL023637, 2005.

Lanz, V. A., Alfarra, M. R., Baltensperger, U., Buchmann, B., Hueglin, C. and Prevot, A. S. H.: Source apportionment of submicron organic aerosols at an urban site by factor analytical modelling of aerosol mass spectra, Atmos. Chem. Phys., 1503–1522, 2007.

Lighty, J. S., Veranth, J. M. and Sarofim, A. F.: Combustion Aerosols: Factors Governing Their Size and Composition and Implications to Human Health, J. Air Waste Manage. Assoc., 50(9), 1565–1618, doi:10.1080/10473289.2000.10464197, 2000.

Liu, L., Lacis, A.A., Carlson, B. E., Mishchenko, M. I. and Cairns, B.: Assessing Goddard Institute for Space Studies ModelE aerosol climatology using satellite and ground-based measurements: A comparison study, J. Geophys. Res., 111(D20), D20212, doi:10.1029/2006JD007334, 2006.

Matthew, B. M., Middlebrook, A. M. and Onasch, T. B.: Collection Efficiencies in an Aerodyne Aerosol Mass Spectrometer as a Function of Particle Phase for Laboratory Generated Aerosols, Aerosol Sci. Technol., 42(11), 884–898, doi:10.1080/02786820802356797, 2008.

Minguillón, M. C., Perron, N., Querol, X., Szidat, S., Fahrni, S. M., Alastuey, A., Jimenez, J. L., Mohr, C., Ortega, A. M., Day, D. A., Lanz, V. A., Wacker, L., Reche, C., Cusack, M., Amato, F., Kiss, G., Hoffer, A., Decesari, S., Moretti, F., Hillamo, R., Teinilä, K., Seco, R., Peñuelas, J., Metzger, A., Schallhart, S., Müller, M., Hansel, A., Burkhart, J. F., Baltensperger, U., and Prévôt, A. S. H.: Fossil versus contemporary sources of fine elemental and organic carbonaceous particulate matter during the DAURE campaign in Northeast Spain, Atmos. Chem. Phys., 11, 12067-12084, doi:10.5194/acp-11-12067-2011, 2011.

Mohr, C., Huffman, J. A., Cubison, M. J., Aiken, A. C., Kenneth, S., Kimmel, J. R., Ulbrich, I. M., Hannigan, M. and Jimenez, J. L.: Characterization of Primary Organic Aerosol Emissions from Meat Cooking , Trash Burning , and Motor Vehicles with High-Resolution Aerosol Mass Spectrometry and Comparison with Ambient and Chamber Observations Characterization of Primary Organic Aerosol, Environ. Sci. and Tech., 2009.

Ng, N. L., Kroll, J. H., Chan, A. W. H., Chhabra, P. S., Flagan, R. C. and Seinfeld, J. H.: and Physics Secondary organic aerosol formation from m -xylene , toluene , and benzene, , (3), 3909–3922, 2007.

1070 Ng, N. L., Kwan, A. J., Surratt, J. D., Chan, A. W. H., Chhabra, P. S., Sorooshian, A., Pye, H. O. T., Crounse, J.
1071 D., Wennberg, P. O., Flagan, R. C. and Seinfeld, J. H.: Secondary organic aerosol (SOA) formation from
1072 reaction of isoprene with nitrate radicals (NO_3), Atmos. Chem. Phys., 8(14), 4117–4140, doi:10.5194/acp-8-
1073 4117-2008, 2008.

1074 Nordin, E. Z., Eriksson, a. C., Roldin, P., Nilsson, P. T., Carlsson, J. E., Kajos, M. K., Hellén, H., Wittbom, C.,
1075 Rissler, J., Löndahl, J., Swietlicki, E., Svenningsson, B., Bohgard, M., Kulmala, M., Hallquist, M. and Pagels, J.
1076 H.: Secondary organic aerosol formation from idling gasoline passenger vehicle emissions investigated in a
1077 smog chamber, Atmos. Chem. Phys., 13(12), 6101–6116, doi:10.5194/acp-13-6101-2013, 2013.

1078 Parrish, D. D., Stohl, A., Forster, C., Atlas, E. L., Blake, D. R., Goldan, P. D., Kuster, W. C. and de Gouw, J. A.:
1079 Effects of mixing on evolution of hydrocarbon ratios in the troposphere, J. Geophys. Res. Atmos., 112(D10),
1080 doi:10.1029/2006JD007583, 2007.

1081 Platt, S. M., El Haddad, I., Zardini, A.A., Clairotte, M., Astorga, C., Wolf, R., Slowik, J. G., Temime-Roussel,
1082 B., Marchand, N., Ježek, I., Drinovec, L., Močnik, G., Möhler, O., Richter, R., Barmet, P., Bianchi, F.,
1083 Baltensperger, U. and Prévôt, a. S. H.: Secondary organic aerosol formation from gasoline vehicle emissions in a
1084 new mobile environmental reaction chamber, Atmos. Chem. Phys., 13(18), 9141–9158, doi:10.5194/acp-13-
1085 9141-2013, 2013.

1086 Polo-Rehn, L.: Caractérisation des polluants dus au transport routier : Apports méthodologiques et cas d'études
1087 en Rhône Alpes, PhD thesis, Grenoble Univ., 2013.

1088 Presto, A. A., Miracolo, M. A., Donahue, N. M. and Robinson, A. L.: Secondary Organic Aerosol Formation
1089 from High-NOx Photo-Oxidation of Low Volatility Precursors: n-Alkanes, Environ. Sci. Technol., 44(6), 2029–
1090 2034, doi:10.1021/es903712r, 2010.

1091 Russell, L. M., Bahadur, R. and Ziemann, P. J.: Identifying organic aerosol sources by comparing functional
1092 group composition in chamber and atmospheric particles., Proc. Natl. Acad. Sci. U. S. A., 108(9), 3516–21,
1093 doi:10.1073/pnas.1006461108, 2011.

1094 Saarikoski, S., Carbone, S., Decesari, S., Giulianelli, L., Angelini, F., Canagaratna, M., Ng, N. L., Trimborn, a.,
1095 Facchini, M. C., Fuzzi, S., Hillamo, R. and Worsnop, D.: Chemical characterization of springtime
1096 submicrometer aerosol in Po Valley, Italy, Atmos. Chem. Phys., 12(18), 8401–8421, doi:10.5194/acp-12-8401-
1097 2012, 2012.

1098 Shilling, J. E., Zaveri, R.A., Fast, J. D., Kleinman, L., Alexander, M. L., Canagaratna, M. R., Fortner, E., Hubbe,
1099 J. M., Jayne, J. T., Sedlacek, a., Setyan, a., Springston, S., Worsnop, D. R. and Zhang, Q.: Enhanced SOA
1100 formation from mixed anthropogenic and biogenic emissions during the CARES campaign, Atmos. Chem.
1101 Phys., 13(4), 2091–2113, doi:10.5194/acp-13-2091-2013, 2013.

1102 Stroud, C. A., Moran, M. D., Makar, P. A., Gong, S., Gong, W., Zhang, J., Slowik, J. G., Abbatt, J. P. D., Lu, G.,
1103 Brook, J. R., Mihele, C., Li, Q., Sills, D., Strawbridge, K. B., McGuire, M. L. and Evans, G. J.: Evaluation of
1104 chemical transport model predictions of primary organic aerosol for air masses classified by particle component-
1105 based factor analysis, Atmos. Chem. Phys., 12(18), 8297–8321, doi:10.5194/acp-12-8297-2012, 2012.

1106 Sun, Y. L., Zhang, Q., Schwab, J. J., Chen, W.-N., Bae, M.-S., Hung, H.-M., Lin, Y.-C., Ng, N. L., Jayne, J.,
1107 Massoli, P., Williams, L. R. and Demerjian, K. L.: Characterization of near-highway submicron aerosols in New
1108 York City with a high-resolution aerosol mass spectrometer, Atmos. Chem. Phys., 12(4), 2215–2227,
1109 doi:10.5194/acp-12-2215-2012, 2012.

1110 Sun, Y., Zhang, Q., Zheng, M., Ding, X., Edgerton, E. S. and Wang, X.: Characterization and source
1111 apportionment of water-soluble organic matter in atmospheric fine particles (PM2.5) with high-resolution
1112 aerosol mass spectrometry and GC-MS., Environ. Sci. Technol., 45(11), 4854–61, doi:10.1021/es200162h,
1113 2011.

1114 Thornhill, D. A., Williams, A. E., Onasch, T. B., Wood, E., Herndon, S. C., Kolb, C. E., Knighton, W. B.,
1115 Zavala, M., Molina, L. T. and Marr, L. C.: Application of positive matrix factorization to on-road measurements
1116 for source apportionment of diesel- and gasoline-powered vehicle emissions in Mexico City, Atmos. Chem.
1117 Phys., 10(8), 3629–3644, doi:10.5194/acp-10-3629-2010, 2010.

1118 Ulbrich, I. M., Canagaratna, M. R., Zhang, Q., Worsnop, D. R. and Jimenez, J. L.: Interpretation of organic
1119 components from Positive Matrix Factorization of aerosol mass spectrometric data, Atmos. Chem. Phys., 9(9),
1120 2891–2918, doi:10.5194/acp-9-2891-2009, 2009.

1121 Vestreng, V., Ntziachristos, L., Semb, A., Reis, S., Isaksen, I. S. A. and Tarras, L.: Evolution of NOx emissions
1122 in Europe with focus on road transport control measures, Atmos. Chem. Phys., 1503–1520, 2009.

1123 WHO: Health Effects of Particulate Matter: Policy imlications for countries in eastern Europe, Caucasus and
1124 central Asia, World Health. Organ., 15 [online] Available from: www.euro.who.int, 2013.

1125 World Bank: World Development Report 2011: World Development Indicators, Fossil Fuel Energy
1126 Consumption., 2011.

1127 Xu, J., Zhang, Q., Chen, M., Ge, X., Ren, J. and Qin, D.: Chemical composition, sources, and processes of urban
1128 aerosols during summertime in Northwest China: insights from High Resolution Aerosol Mass Spectrometry,
1129 Atmos. Chem. Phys. Discuss., 14(11), 16187–16242, doi:10.5194/acpd-14-16187-2014, 2014.

1130 Zhang, Q., Worsnop, D. R., Canagaratna, M. R. and Jimenez, J.-L.: Hydrocarbon-like and oxygenated organic
1131 aerosols in Pittsburgh: insights into sources and processes of organic aerosols, Atmos. Chem. Phys. Discuss.,
1132 5(5), 8421–8471, doi:10.5194/acpd-5-8421-2005, 2005.

1133
1134
1135